**UNIVERSIDADE PAULISTA**

**PROGRAMA DE PÓS-GRADUAÇÃO EM ODONTOLOGIA**

# REGULAÇÃO EPIGENÉTICA DE FATORES DE TRANSCRIÇÃO OSTEOGÊNICOS EM CÉLULAS DO LIGAMENTO PERIODONTAL – UM ESTUDO *IN VITRO* E *IN SILICO*.

Tese apresentada ao Programa de Pós-graduação em Odontologia da Universidade Paulista – UNIP, como requisito para obtenção do título de Doutor em Odontologia.

**ROGÉRIO SALINAS FERREIRA**

**SÃO PAULO**

**2023**

**UNIVERSIDADE PAULISTA**

**PROGRAMA DE PÓS-GRADUAÇÃO EM ODONTOLOGIA**

# REGULAÇÃO EPIGENÉTICA DE FATORES DE TRANSCRIÇÃO OSTEOGÊNICOS EM CÉLULAS DO LIGAMENTO PERIODONTAL – UM ESTUDO *IN VITRO* E *IN SILICO*.

Tese apresentada ao Programa de Pós-graduação em Odontologia da Universidade Paulista – UNIP, como requisito para obtenção do título de Doutor em Odontologia, sob orientação da Profª. Drª. Denise Carleto Andia.

Área de concentração: Clínica Odontológica.
Subárea: Periodontia.

**ROGÉRIO SALINAS FERREIRA**

**SÃO PAULO**

**2023**

**ROGÉRIO SALINAS FERREIRA**

# REGULAÇÃO EPIGENÉTICA DE FATORES DE TRANSCRIÇÃO OSTEOGÊNICOS EM CÉLULAS DO LIGAMENTO PERIODONTAL – UM ESTUDO *IN VITRO* E *IN SILICO*.

Tese apresentada ao Programa de Pós-graduação em Odontologia da Universidade Paulista – UNIP, como requisito para obtenção do título de Doutor em Odontologia.

Aprovado em: ___/___/___

BANCA EXAMINADORA

_____ - __/__/__
Prof. Dr. Rodrigo Almeida da Silva
Universidade Paulista – UNIP

_____ - __/__/__
Profª. Drª. Denise Carleto Andia
Universidade Paulista – UNIP

_____ - __/__/__
Profª. Drª. Rahyza Inacio Freire de Assis
Universidade Federal do Espírito Santo – UFES

_____ - __/__/__
Profª. Drª. Emanuella Prado Ferraz
Universidade de São Paulo – USP

_____ - __/__/__
Prof. Dr. Márcio Mateus Beloti
Universidade de São Paulo – USP

## DEDICATÓRIA

Dedico este trabalho, primeiramente, ao meu Deus, Senhor e Salvador JESUS CRISTO, pela dádiva da vida, pelo sustento e fortalecimento durante toda essa caminhada. Aos meus pais, Antônia de Lourdes Salinas Ferreira e José Djalma Ferreira (*in memoriam*), à minha esposa, Monica Venturineli Ferreira, e à minha filha, Gabriela Venturineli Ferreira, que são meus exemplos e fonte de força e inspiração.

## AGRADECIMENTOS

Às três mulheres da minha vida: minha mãe, minha esposa e minha filha, pelo apoio constante para que eu pudesse seguir na busca por este sonho, por acreditarem no meu potencial; pelas palavras de motivação nos momentos de desânimo e principalmente por terem sacrificado momentos de lazer e descanso para que eu pudesse me dedicar a este trabalho.

Aos meus familiares, especialmente ao meu irmão Tiago Salinas Ferreira, por sempre torcer pelas minhas conquistas.

À minha orientadora Profª. Drª. Denise Carleto Andia, por ter me introduzido e guiado nesse fascinante "mundo da epigenética", por toda paciência e dedicação durante esse meu aprendizado, pela confiança no meu trabalho, por ter sido muito mais do que um exemplo de excelência acadêmica, mas um exemplo de ser humano generoso e motivador.

Aos professores do Programa de Pós-graduação em Odontologia da UNIP, por toda ajuda, toda atenção e todos os conselhos dados durante essa jornada e por compartilharem não apenas seus conhecimentos, mas também suas experiências e vivências, graças aos quais posso ser hoje uma pessoa melhor.

Aos meus amigos de pós-graduação, especialmente à Nathália Prado e à Tayná Castro, pela parceria sempre acompanhada de um café e muita risada, tornando os dias mais leves e alegres, pelas conversas descontraídas, mas sempre construtivas, e pelas palavras e ações de apoio.

À nossa equipe de projeto e pesquisa, especialmente à Profª. Drª. Rahyza Freire de Assis e ao Prof. Dr. Rodrigo Augusto da Silva, por todos os ensaios laboratoriais realizados e por todo auxílio na redação e revisão deste trabalho.

Aos funcionários da UNIP, por toda gentileza e ajuda nas tarefas diárias.

À UNIP – Universidade Paulista, pelo apoio e suporte.

À Coordenação de Aperfeiçoamento de Pessoal de Nível Superior (CAPES), pelo auxílio financeiro para a minha bolsa de Doutorado.

*“Nada aquém do meu melhor e nada além do meu possível.”*

*(autoria própria)*

## RESUMO

Este estudo *in vitro* e *in silico* teve como objetivo investigar os mecanismos epigenéticos que regulam o perfil (pós)transcricional dos fatores de transcrição (TFs) osteogênicos *Sp7 Transcription Factor* (SP7) e *Distal-Less Homeobox* 4 (DLX4), além da correlação de expressão gênica entre a histona desmetilase *JARID1B* e o TF osteogênico *Runt-related transcription factor 2* (RUNX2), em células mesequimais do ligamento periodontal humano com alta (h-PDLCs) e baixa (l-PDLCs) capacidade de deposição mineral. As populações celulares foram cultivadas em meios de cultura com e sem indução osteogênica (OM e DMEM, respectivamente), durante os períodos de 3 e 10 dias. Após cada período de cultura celular, foram realizadas as extrações do DNA, RNA e proteínas, sendo esse material obtido submetido às técnicas de ATAC-seq, Metiloma, RNA-seq, PCR e *Western-Blotting*. Os dados foram processados e analisados por programas e ferramentas de bioinformática baseados em ambientes *R*, *Python* e *webserver*. As análises do ATAC-seq apontaram as regiões genômicas de *SP7* e *DLX4* mais acessíveis nas l-PDLCs quando comparadas às h-PDLCs. Nas análises do Metiloma, esses TFs apresentaram padrões de metilação diferentes entre si, mas sem sondas diferencialmente metiladas (DMPs) entre l- e h-PDLCs. O padrão de metilação da *JARID1B* foi menor nas l-PDLCs, em ambos os períodos avaliados (3 e 10 dias). As análises de RNA-seq mostraram *SP7* e *DLX4* diferencialmente menos expressos nas l-PDLCs, tanto no DMEM quanto no OM. Os RNAs longos não codificantes (lncRNAs) *MIR31HG* e *LINC00939* foram achados diferencialmente mais expressos em ambas as condições de l-PDLCs. O programa de predição *RIblast*, baseado no webserver *LncRRIsearch*, previu interações de pareamento de bases (RNA:RNA) entre transcritos de *SP7*, *DLX4*, *MIR31HG* e *LINC00939*. O programa de aprendizado de máquina *TriplexFPP* previu potencial de formação triplex (DNA:RNA) para *SP7* e para *LINC00939*. Os resultados de PCR e *Western-Blotting* mostraram níveis aumentados de JARID1B nas l-PDLCs (x h-PDLCs), com correlações negativas de expressão com *RUNX2*. Juntos, esses resultados indicam a histona desmetilase JARID1B e os lncRNAs MIR31HG e LINC00939 como possíveis reguladores epigenéticos no comprometimento osteogênico das l-PDLCs.



Palavras-chaves: Epigenética; Osteogênese; Células-Tronco Mesenquimais; Ligamento Periodontal

## ABSTRACT

The aim of this *in vitro* and *in silico* was to investigate the epigenetic mechanisms that regulate the (post)transcriptional profile of the osteogenic transcription factors (TFs) *Sp7 Transcription Factor* (SP7) and *Distal-Less Homeobox* 4 (DLX4), in addition to the correlation of gene expression between the histone demethylase JARID1B and the osteogenic TF *Runt-related transcription factor 2* (RUNX2), in periodontal ligament stem-cells with high (h-PDLCs) and low (l-PDLCs) capacity for mineral deposition. The populations were cultivated in culture media with and without osteogenic induction (OM and DMEM, respectively), during periods of 3 and 10 days. After each culture period, DNA, RNA and protein were extracted from these cells, and this material obtained was submitted to the ATAC-seq, Methylome, RNA-seq, PCR and Western-Blotting techniques. Data were processed and analyzed by bioinformatics programs and tools based on *R*, *Python* and webserver environments. ATAC-seq analyzes indicated the genomic regions of *SP7* and *DLX4* more accessible in l-PDLCs when compared to h-PDLCs. In the Methylome analyses, these TFs showed different methylation patterns among themselves, but without differentially methylated probes (DMPs) between l- and h-PDLCs. The *JARID1B* methylation pattern was also analyzed, which was less methylated in l-PDLCs, in both culture periods (3 and 10 days). RNA-seq analyzes showed *SP7* and *DLX4* differentially less expressed in both culture conditions (DMEM and OM) on l-PDLCs. The long non-coding RNAs (lncRNAs) MIR31HG and LINC00939 were found differentially more expressed in both l-PDLC conditions. The *RIblast* prediction program, based on the *LncRRIsearch* webserver, predicted base-pairing (RNA:RNA) interactions between SP7, DLX4, MIR31HG and LINC00939 transcripts. The *TriplexFPP* machine learning program predicted potential for triplex formation (DNA:RNA) for *SP7* and for LINC00939. PCR and Western-Blotting results showed reduced levels of JARID1B in h-PDLCs compared to l-PDLCs, and inversely proportional expression correlations with *RUNX2(p57)*. Together, these results indicate the histone demethylase JARID1B and the lncRNAs MIR31HG and LINC00939 as possible epigenetic regulators in the osteogenic commitment of the l-PDLCs.



Keywords: Epigenetic; Osteogenesis; Mesenchymal Stem Cells, Periodontal Ligament

**SUMÁRIO**

## 1. INTRODUÇÃO

A reabsorção óssea alveolar, seja de origem fisiológica, patológica ou traumática, é considerada um desafio na Odontologia, principalmente para a preservação e manutenção, tanto dos dentes naturais quanto dos implantes osseointegrados[1]. As abordagens utilizadas no combate desse problema, vão desde o emprego de estratégias preventivas, como a orientação e promoção da higiene oral, até as intervenções não-cirúrgicas e cirúrgicas, como o aplainamento radicular e as regenerações ósseas guiadas (ROGs), respectivamente[2-4].

As ROGs podem ser associadas à aplicação de células mesenquimais indiferenciadas (*mesenchymal stem-cells*, MSCs)[5,6], que são capazes de se diferenciar em múltiplas linhagens fenotípicas, inclusive a osteogênica, fundamental na reparação óssea alveolar[7]. Na cavidade oral, as MSCs podem ser obtidas em diversos nichos, como em dentes decíduos exfoliados (*stem-cells from human exfoliated deciduous teeth*, SHED), polpa dental (*dental pulp stem-cells*, DPSCs), gengiva (*gingival-derived mesenchymal stem-cells*, GMSCs) e ligamento periodontal (*periodontal ligament stem-cells*, PDLSCs)[8].

As PDLCs são capazes de se diferenciar em células osteogênicas[9], porém podem apresentar potenciais de deposição mineral distintos, *in vitro*: alto potencial (*high potential PDLCs*, h-PDLCs) e baixo potencial (*low potential PDLCs*, l-PDLCs)[10], o que pode comprometer os resultados das ROGs. Essa heterogeneidade é determinada, entre outros aspectos, pela regulação epigenética dos fatores de transcrição (*transcriptional factors*, TFs), que são proteínas que se ligam ao DNA e induzem a diferenciação fenotípica celular[11]. Os principais TFs envolvidos na diferenciação osteogênica são o RUNX2 (*Runt-related Transcription Factor 2*), ATF4 (*Activating Transcription Factor 4*), MSX2 (*Msh Homeobox 2*), SATB2 (*SATB Homeobox 2*), CTNNB1 (*Catenin Beta 1*) e SP7 (*Sp7 Transcription Factor*), além das famílias DLX (*Distal-Less Homeobox*) e TWIST (*Twist Family BHLH Transcription Factor*)[12]. Em estudo prévio do nosso grupo[11], os TFs SP7 e DLX4 foram encontrados diferencialmente expressos entre as PDLCs (h- e l-).

A regulação epigenética é dada pelo conjunto de interações intermoleculares entre o genoma/transcriptoma e os agentes reguladores, como as HDMs (*Histone Demethylase*), as DNMTs (*DNA methyltransferases*) e os ncRNAs (*non-coding*

*RNAs*)[13]. As HDMs podem inibir a transcrição dos TFs através da desmetilação nos resíduos de lisina das histonas, promovendo a condensação da cromatina (heterocromatina) e, consequentemente, impedir o acesso das DNA polimerases[14]. Uma das principais HDMs envolvidas na osteogênese é a JARID1B[15]. Inversamente, as DNMTs silenciam o processo transcricional adicionando um grupo metil diretamente sobre o carbono 5 da citosina, formando o complexo 5-metilcitosina (5mC), promovendo a hipermetilação do DNA[16].

Os ncRNAs podem ser classificados de acordo com a quantidade de nucleotídeos: curtos (*microRNAs*, miRNAs), com aproximadamente 22 nucleotídeos, e longos (*long non-coding RNAs*, lncRNAs), com mais de 200 nucleotídeos. Os miRNAs podem atuar principalmente como silenciadores pós-transcricionais dos TFs, promovendo a degradação dos seus mRNAs através do RISC (*RNA-induced silencing complex*)[17]. Os lncRNAs, por sua vez, regulam os processos (pós)transcricionais dos TFs através do pareamento de bases entre lncRNA-*DNA* e lncRNA-RNA, entre outros mecanismos[18].

Diante disso, o objetivo desse estudo foi analisar a regulação epigenética dos principais fatores de transcrição envolvidos na diferenciação osteogênica de PDLCs com diferentes potenciais de deposição mineral, através de ensaios *in vitro* e *in silico*.

## 2. ARTIGO 1 (PUBLICADO NA REVISTA *GENES*)

genes

MDPI

*Article*

# Analyzes In Silico Indicate the lncRNAs MIR31HG and LINC00939 as Possible Epigenetic Inhibitors of the Osteogenic Differentiation in PDLCs

**Rogério S. Ferreira [1], Rahyza I. F. Assis [2], Francesca Racca [3], Ana Carolina Bontempi [1], Rodrigo A. da Silva [4], Malgorzata Wiench [5,*] and Denise C. Andia [1,*]**

1 School of Dentistry, Health Science Institute, Paulista University, São Paulo 04026-002, SP, Brazil; rogerio.ferreira25@aluno.unip.br (R.S.F.); anacarolina.bontempi@gmail.com (A.C.B.)
2 Department of Clinical Dentistry, Federal University of Espírito Santo, Vitória 29043-910, ES, Brazil
3 Periodontology Department, The Ohio State University College of Dentistry, Columbus, OH 43210-1267, USA; francesca_racca@hotmail.com
4 Program in Environmental and Experimental Pathology, Paulista University, São Paulo 04026-002, SP, Brazil; dasilva.rodrigo.a@gmail.com
5 School of Dentistry, Institute of Clinical Sciences, Institute of Cancer and Genomic Sciences, University of Birmingham, Birmingham B5 7EG, UK
* Correspondence: m.d.wiench@bham.ac.uk (M.W.); denise.andia@docente.unip.br (D.C.A.)

**Abstract:** Chromatin conformation, DNA methylation pattern, transcriptional profile, and non-coding RNAs (ncRNAs) interactions constitute an epigenetic pattern that influences the cellular phenotypic commitment and impacts the clinical outcomes in regenerative therapies. Here, we investigated the epigenetic landscape of the SP7 transcriptor factor (*SP7*) and Distal-Less Homeobox 4 (*DLX4*) osteoblastic transcription factors (TFs), in human periodontal ligament mesenchymal cells (PDLCs) with low (l-PDLCs) and high (h-PDLCs) osteogenic potential. Chromatin accessibility (ATAC-seq), genome DNA methylation (Methylome), and RNA sequencing (RNA-seq) assays were performed in l- and h-PDLCs, cultured at 10 days in non-induced (DMEM) and osteogenic (OM) medium in vitro. Data were processed in *HOMER*, *Genome Studio*, and *edgeR* programs, and metadata was analyzed by online bioinformatics tools and in *R* and *Python* environments. ATAC-seq analyses showed the TFs genomic regions are more accessible in l-PDLCs than in h-PDLCs. In Methylome analyses, the TFs presented similar average methylation intensities (AMIs), without differently methylated probes (DMPs) between l- and h-PDLCs; in addition, there were no differences in the expression profiles of TFs signaling pathways. Interestingly, we identified the long non-coding RNAs (lncRNAs), *MIR31HG* and *LINC00939*, as upregulated in l-PDLCs, in both DMEM and OM. In the following analysis, the web-based prediction tool *LncRRIsearch* predicted RNA:RNA base-pairing interactions between *SP7*, *DLX4*, *MIR31HG*, and *LINC00939* transcripts. The machine learning program *TriplexFPP* predicted DNA:RNA triplex-forming potential for the *SP7* DNA site and for one of the LINC00939 transcripts (*ENST00000502479*). PCR data confirmed the upregulation of *MIR31HG* and *LINC00939* transcripts in l-PDLCs (× h-PDLCs) in both DMEM and OM ($p < 0.05$); conversely, *SP7* and *DLX4* were downregulated, confirming those results observed in the RNA-Seq analysis. Together, these results indicate the lncRNAs MIR31HG and LINC00939 as possible epigenetic inhibitors of the osteogenic differentiation in PDLCs by (post)transcriptional and translational repression of the *SP7* and *DLX4* TFs.

**Keywords:** PDLC; epigenetic; osteogenic; SP7; DLX4; MIR31HG; LINC00939



**Citation:** Ferreira, R.S.; Assis, R.I.F.; Racca, F.; Bontempi, A.C.; da Silva, R.A.; Wiench, M.; Andia, D.C. Analyzes In Silico Indicate the lncRNAs MIR31HG and LINC00939 as Possible Epigenetic Inhibitors of the Osteogenic Differentiation in PDLCs. *Genes* **2023**, *14*, 1649. https://doi.org/10.3390/genes14081649

Academic Editors: Naila Francis Paulo De Oliveira and Maria Cristina Leme Godoy dos Santos

Received: 16 July 2023
Revised: 10 August 2023
Accepted: 14 August 2023
Published: 18 August 2023



## 1. Introduction

Over the past decades, stem cell-based treatment associated with regenerative therapies has become increasingly promising for the treatment of several diseases such as diabetes, cardiac ischemia, and osteoarthritis [1]. Mesenchymal stem cells (MSCs) can

be obtained from several sources, such as bone marrow (BMSCs), adipose tissue (ASCs), peripheral blood (HSCs) [2], and teeth (periodontal ligament cells—PDLCs, dental pulp cells—DPCs, and stem cell from exfoliated human dentition—SHED) [3]. MSCs are characterized by self-renewing, differentiation into cell multilineages capacities, and specific surface markers [4]. Moreover, MSCs show inherent tropism toward damaged tissues and the ability to regenerate them [5,6].

PDLCs can differentiate into osteoblastic, adipocyte, neuronal, and chondrogenic-like cells [7], although they might present distinct capacities to produce mineral nodules in vitro [8–12], which could impact clinical applications. This heterogeneity may be related to cell fate commitment, which is "the commitment of cells to specific cell fates and their capacity to differentiate into particular kinds of cells" (Gene_Ontology_Term_Definition_GO:0045165).

The cell fate commitment is determined by lineage-specific transcription factors (TFs), which are proteins that bind in DNA sites and drive the cellular phenotype acquisition [13]. These TFs are expressed through signaling pathways, which are cascades of extra and intracellular molecular events that culminate in the TFs gene expression. This entire molecular process is regulated by epigenetic mechanisms such as chromatin conformation, DNA methylation marks, and non-coding RNA (ncRNAs) interferences. Chromatin can remodel into a more condensed (heterochromatin) or less condensed (euchromatin) structure, determining the degree of RNA polymerase accessibility, responsible for gene transcription, at the DNA strand [14]. This conformation is modulated by epigenetic modifications in histones and DNA methylation patterns. The DNA methylation patterns, in turn, are determined by the intensity of the methyl group aggregation at carbon 5 of cytosine (5 mC) [15], favoring or not binding TFs in gene promoter regions [16]. ncRNAs are RNA molecules that are not translated into protein and can be distinguished according to their size: microRNAs (miRNAs), about 22 nucleotides long, and long non-coding RNAs (lncRNAs), over 200 nucleotides long. Mostly, the miRNAs act through RNA-induced silencing complex (RISC) as post-transcriptional silencers, promoting mRNA degradation by the cleavage mechanism or inhibiting its translation by the base pairing mechanism [17]. The lncRNAs can act as transcriptional regulators by the DNA:RNA triple-helix (triplex) forming, through Hoogsteen or reverse Hoogsteen base pairing, i.e., when a polypurine (A–G) or pyrimidine (C–U) motif of an lncRNA interacts with the major groove of a Watson–Crick double-stranded DNA (dsDNA), forming triplets of canonical bases, such as C•G–C and U•A–T (where '•' and '–' represent Hoogsteen and Watson–Crick interactions, respectively) [18,19]. In addition, they can also act as post-transcriptional and translational regulators by the RNA:RNA duplex intermolecular hybridization through nucleotide base pairing interactions between a lncRNA and an mRNA [20], among other mechanisms. However, such mechanisms remain poorly understood.

Previous studies from our group have demonstrated the individual epigenetic profile influences the capacity of extracellular matrix deposition, and, consequently, the osteogenic phenotype acquisition [9,11]; in addition, we also highlighted the *Sp7 Transcription Factor* (*SP7*) and *Distal-Less Homeobox 4* (*DLX4*) genes, key TFs involved in osteoblastic differentiation, as downregulated in PDLCs with a low capacity of mineral matrix deposition [12]. Here, our aim is to investigate, in silico, the epigenetic landscape of both TFs, *SP7*, and *DLX4*, in PDLCs showing the distinct capacity of mineral matrix deposition in vitro.

## 2. Material and Methods

### *2.1. Cell Acquisition and Culture*

After signing an informed consent approved by the Ethics Committee of Piracicaba Dental School, University of Campinas (CAAE55588816.4.0000.5418), PDLCs were collected, isolated, and cultured as described by Silverio et al., 2010 [21]. Then, PDLCs were characterized into low (l-PDLCs) and high osteogenic potential (h-PDLCs), according to their capacity of mineral deposition, in vitro, and according to our previous publications [9–12]. Briefly, PDLCs were characterized according to Dominici et al. [4] to confirm the ability

to differentiate into osteogenic and adipogenic cell lineages and the expression/lack of expression of specific cell surface markers, such as CD166, CD34, and CD45 [22]. The levels of CD34 and CD45 were very similar between h- and l-PDLCs, showing less than 1% of the expression of positive cells. Regarding multipotency marker CD166, more than 95% of cells in both populations showed positive expressions [9–12]. Alizarin red staining was performed to assess the amount of mineral matrix produced in vitro by each cell population [10]. Consequently, PDLCs were classified either as high osteogenic potential PDLCs (h-PDLCs), which was the cell population with the capacity to produce higher amounts of the mineral matrix or low osteogenic potential PDLCs (l-PDLCs with a lower capacity to produce mineral matrix). Based on our previous studies [10,12], we chose day 10 of the osteogenic media (OM) induction as the time point to analyze epigenomic and transcriptomic changes. l- and h-PDLCs were cultured in high glucose Dulbecco's Modified Eagle Medium (DMEM), 10% Fetal Bovine Serum (FBS), 100 U/mL of penicillin, and 100 mg/mL of streptomycin and maintained at 37 °C in a humidified atmosphere containing 5% $CO_2$. Three independent experiments were performed for each PDLC, with three technical replicates for each one, with cells in the passages P5-P8, except when stated otherwise.

### 2.2. Osteogenic Stimulation

Both l- and h-PDLCs were seeded into 6-well plates ($2.5 \times 10^5$ cells/well) in DMEM, 10% FBS, and antibiotics. After 24 h of incubation, for cell adhesion, the culture medium was removed, and the cells were cultivated in non-induced medium (DMEM) supplemented with 10% FBS and 1% antibiotics (penicillin 100 U/mL and streptomycin 100 mg/mL) or in induced osteogenic medium (OM) with DMEM, 10% FBS, 1% antibiotics, and supplemented with ascorbic acid (50 µg/mL), β-glycerophosphate (10 mM), and dexamethasone (10 nM). Cells were incubated and collected after 10 days, with media change every three days. PDLCs were divided according to the following groups:

(i) l-DMEM: l-PDLCs cultivated in DMEM, standard medium.
(ii) l-OM: l-PDLCs cultivated in OM, osteogenic medium.
(iii) h-DMEM: h-PDLCs cultivated in DMEM, standard medium.
(iv) h-OM: h-PDLCs cultivated in OM, osteogenic medium.

For all comparisons, the h-DMEM was set as the control group x l-DMEM, and the h-OM was set as the control group x l-OM.

### 2.3. Assay for Transposase-Accessible Chromatin Using Sequencing (ATAC-Seq)

A total of $5 \times 10^4$ cells were harvested from each group and were incubated in a transposition reaction, as preconized by Buenrostro et al. [23]. The Tn5 transposase enzyme was used to insert an adapter sequence into the accessible chromatin regions, combined with single-step library digestion and preparation. Digitonin was included to reduce contamination with mitochondrial DNA [24]. Then, the transposase-containing DNA fragments were amplified by PCR and purified to select the appropriate size of the fragments. Sample quality was evaluated by TapeStation, quantified by PCR with the Kapa Sybr Fast LightCycler 480 kit, and pooled for subsequent sequencing at Illumina NextSeq 500 platform (Illumina Inc., Foster City, CA, USA) in the Genomics Birmingham Facility (Birmingham, UK). Two independent experiments were performed.

### 2.4. Global DNA Methylation Analysis (Methylome)

DNA Isolation and Oxidative Bisulfite Conversion

The groups were cultured ($8.7 \times 10^5$ cells/100 mm dishes) as described above. After 10 days, the culture medium was removed, and the cells were washed two times with PBS and scrapped off in extraction buffer with proteinase K. Total DNA was purified by extraction with phenol/chloroform/isoamyl alcohol and stored at −20 °C. DNA's concentrations and quality were assessed using Qubit (Thermo Fisher Scientific Inc., Rockford, IL, USA) and spectrophotometer (Nanodrop 1000; Nanodrop Technologies LLC, Wilmington, NC,

USA). The oxidative bisulfite conversion reaction was performed according to the protocol described by Assis et al. [12].

### 2.5. RNA Sequencing (RNA-SEQ)

#### 2.5.1. I. RNA Extraction

Cells from all groups were cultivated at $1.5 \times 10^5$ per well in 6-well plate, as previously described. After 10 days, the culture medium of each well from each group was removed, the cells were washed with PBS and scrapped off with TRIzol reagent (Invitrogen, Cat #15596-018, Waltham, MA, USA), according to the manufacturer's recommendation. Total RNA extraction was performed, and RNA samples were treated with DNA-free Turbo solution to remove genomic DNA (Ambion, Cat #1907, Austin, TX, USA). Then, the samples were submitted to integrity and concentration analysis by the Agilent 2100 bioanalyzer, with an RNA Integrity Number (RIN) value greater than 8.

#### 2.5.2. II. RNA Sequencing

The samples were pooled in equal concentration, prepared, and sequenced with Illumina TruSeq Stranded mRNA Sample Prep Kit, according to the manufacturer's instructions, in Illumina NextSeq 500 platform (Illumina Inc., Foster City, CA, USA). Briefly, 1 µg of DNA-free total RNA samples were processed. The mRNA was fragmented and copied into the first strand cDNA, followed by second strand cDNA synthesis. cDNA fragments were submitted to the final repair process, addition of single adenosine base, and adapter ligation. Finally, the processed cDNA was amplified by 15 cycles of PCR to create the cDNA library, which was read on the HiSeq 2500 (v3) sequencer (Illumina, San Diego, CA, USA).

For more details about these genome wide methodologies, please go to Assis et al., 2022.

### 2.6. Bioinformatics Analysis

#### 2.6.1. III. ATAC-Seq

The reads were aligned to the human genome (h19) through the *Bowtie2 tool* [25] and the duplicates were removed. The ENCODE consortium identified the blacklist reads, defined as anomalous. Non-exclusively mapped reads have been filtered and peaks have been called using the "factor mode" in HOMER [26], based on the default settings. A Bigwig file was also generated and uploaded in the UCSC Genome Navigator [22] to allow visualization of the accumulated reads. Analyses using HOMER and subsequent analyses were conducted with the help of Dr. Samuel Clokie (West Midlands Regional Genetics Laboratory, Birmingham Women's Hospital, Birmingham, UK).

#### 2.6.2. IV. DNA Methylome

Epic BeadChips data was processed through Illumina Genome Studio program [27] and minfi [28], implemented in R, associated with dplyr [29] and tidyr [30] packages. Data normalization was performed using quartiles methods. Probes were considered differentially methylated (DMP) when presented values of delta $\beta > 0.2$ (hypermethylated) or $< -0.2$ (hypomethylated) and p-value $< 0.01$. The average methylation intensity (AMI) of the TFs was calculated by the sum of the average β (AVG-β) values of the detected probes (sd), divided by the number of probes:

$$\overline{\text{AMI}} = \frac{\sum AVG\_\beta(sd)}{n(sd)}. \quad (1)$$

The scatter plots representing the annotation, AMI, and AVG-β values and AMI of the TFs probes were generated in Microsoft Excel 365.

#### 2.6.3. RNA-Seq

The reads were aligned to the hg19 reference genome and counted using the R *Rsubread* package [31]. Quantification was performed according to the last recommended pipeline, as defined in the *edgeR* software [32]. Genes were considered differentially expressed (DEGs) when presented values of log2FoldChange (logFC) $\geq 1.5$ (upregulated) or $\leq -1.5$ (downregulated), and $p$-value $\leq 0.05$. "Heatmaps" representing the logFC intensity were generated in *R* environment with the ComplexHeatmap package [33], and the "volcano plots" representing both logFC amplitude and statistical significance (-log10pvalue), with the EnhancedVolcano package [34].

#### 2.6.4. Selection of lncRNAs and Prediction Analyses

The lncRNAs found DEGs (DElncRNAs) were upregulated in common between the RNA-seq datasets of the l-DMEM ($\times$ h-DMEM) and l-OM ($\times$ h-OM) groups and were selected and submitted to prediction analysis for RNA:RNA base-pairing interactions with the TFs, using the RIblast prediction program, based on the LncRRIsearch web server [35]. Since the TruSeq Stranded mRNA Sample Prep Kit, used in RNA Sequencing, is not quite suitable for non-coding RNA without polyA tails, we check if the selected DElncRNAs have polyadenylation sites from 3′ end sequencing, in the PolyASite database [36]. Next, they verified the potentials of DNA:RNA triplex formation of these predicted DElncRNAs and of the TFs, using the TriplexFPP machine learning program, in the Python environment, which (1) predicted the probabilities of triplex-forming oligonucleotide (TFO), in practice, for these DElncRNAs and (2) the potentials triplex target sites (TTSs) on the TFs DNA sequences, based on experimentally verified data, considering positive triplex-forming for score > 0.5 [37]. The FASTA sequences input in the program were obtained in the Ensembl genome browser, under the "Human (GRCh37.p13)" parameter [38]. The pie charts and Venn diagrams representing the distribution of the DElncRNAs among the groups was generated in Microsoft Excel 365 and with the online tool Interactivenn, respectively [39].

### *2.7. PCR Analysis*

cDNA synthesis was performed using 1 mg RNA as described previously [40]. Quantitative polymerase chain reaction (PCR) was carried out for each one of the three independent experiments, using LightCycler 96 Real-Time PCR System (Roche Diagnostics GmbH, Mannheim, Germany) and FastStart Essential DNA Green Master (Roche Diagnostic Co., Indianapolis, IN, USA), according to the manufacturer's instructions and in technical triplicates. The primers' sequences and reaction details are shown in Supplementary Table S1. The results of *MIR31HG*, *LINC00939*, *SP7* and *DLX4* were obtained from three biological replicates, in technical triplicates, analyzed by ΔΔCt method [41] and are presented as relative amounts of the target gene using *18S* as inner reference gene.

### *2.8. Statistical Analysis of the PCR Data*

Data were initially examined for normality by Shapiro–Wilk test and expressed as mean $\pm$ standard deviation (SD). After normal data distribution was confirmed, one-way analysis of variance (ANOVA $\alpha \leq 0.05$) followed by pairwise multiple-comparison test (Tukey) were used to identify the difference amongst groups (GraphPad Prism 7—GraphPad Software Inc., San Diego, CA, USA).

## 3. Results

### *3.1. l-PDLCs Show More Accessible Chromatin Regions in SP7 and DLX4 Genes than h-PDLCs*

The chromatin conformation coordinates the DNA accessibility of the transcriptional machinery, composed of the RNA polymerase II, TFs, among other molecular elements, responsible for gene expression. The chromatin accessibility analysis on *SP7* and *DLX4* genomic regions in both h- and l-PDLCs, induced (h-OM and l-OM) and non-induced (h-DMEM and l-DMEM), to osteogenesis in vitro at 10 days showed more accessible chromatin peaks in l-PDLCs compared to h-PDLCs, in both culture conditions, i.e., induced, and non-

induced (Figure 1). In summary, l-PDLCs exhibit chromatin conformation more favorable to *SP7* and *DLX4* genes transcription than h-PDLCs.

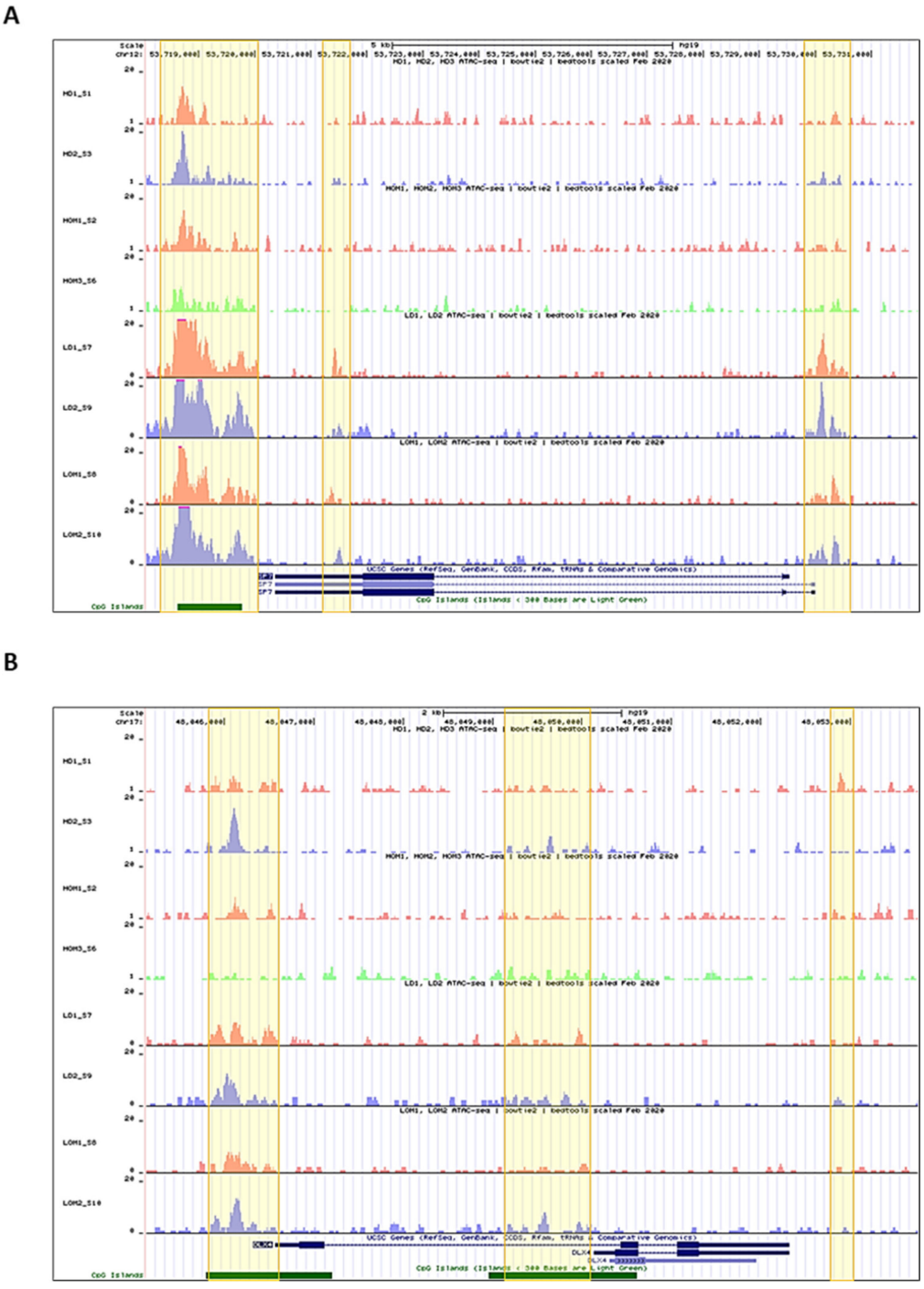


**Figure 1.** Overview of the chromatin accessibility on the *SP7* and *DLX4* gene regions in each h-PDLCs and l-PDLCs sample: The *bigwig* annotation tracks represent the accessible peaks on the *SP7* (**A**) and *DLX4* (**B**) gene regions in each h-PDLCs (DMEM and OM) and l-PDLCs (DMEM and OM) sample. Highlighted in yellow are the genomic regions with higher peak scores. *HD1_S1* and *HD2_S3* = h-DMEM samples; *HOM1_S2* and *HOM3_S6* = h-OM samples; *LD1_S7* and *LD2_S9* = l-DMEM samples; *LOM1_S8* and *LOM2_S20* = l-OM samples.

### *3.2. DNA Methylation Patterns amongst l- and h-PDLCS Are Similar for SP7 and DLX4*

In turn, DNA methylation is one of the main epigenetic mechanisms that regulate chromatin conformation and gene transcription. We investigated the DNA methylation patterns of the *SP7* and *DLX4* genes in the Methylome metadata. Despite the probes presenting different AVG-β values in *SP7* and *DLX4*, the average methylation intensities (AMI) were similar, exhibiting a less methylated pattern, except for the 3′UTR region in *DLX4*, whose AMI pattern was more methylated (Figure 2). No differentially methylated probes (DMPs) were found between l- and h-PDLCs, in both culture conditions. These results reveal similar DNA methylation patterns among *SP7* and *DLX4* (except in the 3′UTR region), without significant differences between l- and h-PDLCs. There were no other found osteogenic TFs or signaling pathways that were differently expressed among l- and h-PDLCs.

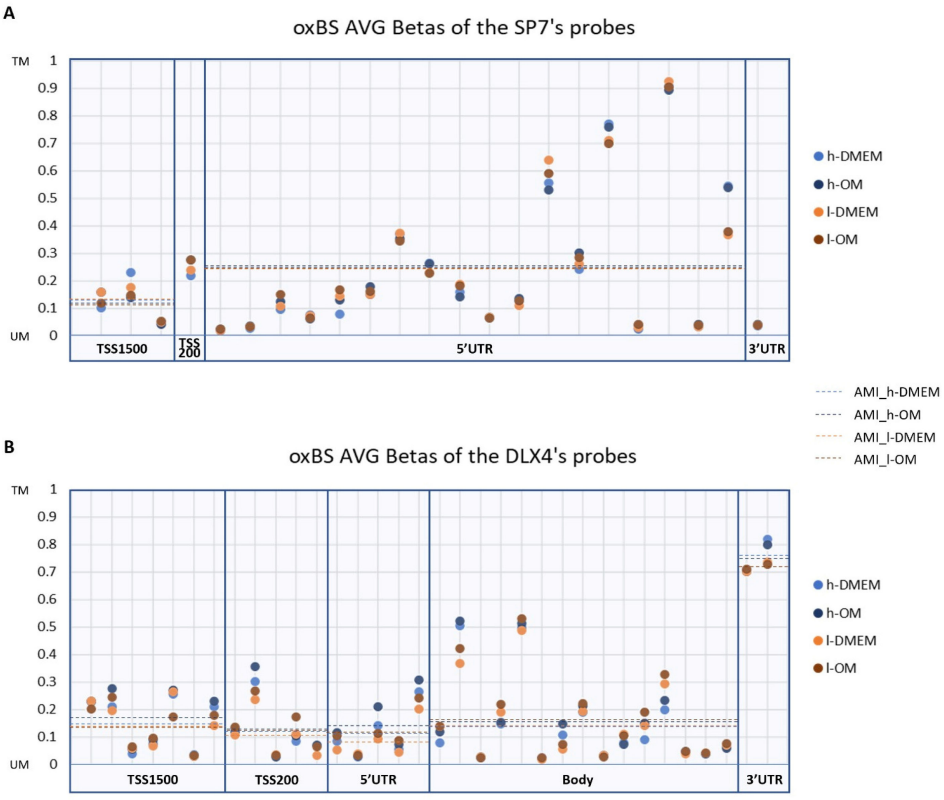


**Figure 2.** DNA methylation patterns in *SP7* and *DLX4* gene regions: The scatter plots represent the average β values (AVG-β) of each probe detected for *SP7* (**A**) and *DLX4* (**B**) gene regions in the oxidative bisulfite sequencing (oxBS) dataset. The dotted lines indicate the average methylation intensity (AMI) of the probes according to *UCSC_RefGene_Group*. TM: Totally Methylated; UM: Unmethylated.

The gene transcription mechanism is the biological consequence of molecular events that occur in extra and intracellular cascades called signaling pathways. Due to the inconsistency observed between the transcriptional profile and the epigenetic background of the TFs *SP7* and *DLX4* in our previous research [12], we analyzed the transcriptional profiles of the main signaling pathways involved in osteogenesis, in the l-DMEM (x h-DMEM), and in the l-OM (x h-OM) RNA-seq dataset. In addition, we analyzed the transcriptional profiles of other osteogenic TFs, like *RUNX2*, *SATB2*, *ATF4*, *MSX2*, *CTNNB1*, *DLX5*, and *TWIST1/2*. No differently expressed genes (DEGs) were found for these TFs (Figure 3A) or signaling pathways, except for *Sclerostin* (*SOST*), a negative regulator of the WNT/β-catenin pathway, founded DEG (downregulated) in both l-PDLCs groups (Figure 3B). This result points to no significant differences in the transcriptional profiles of other osteogenic TFs or signaling pathways between l- and h-PDLCs, in both culture conditions.

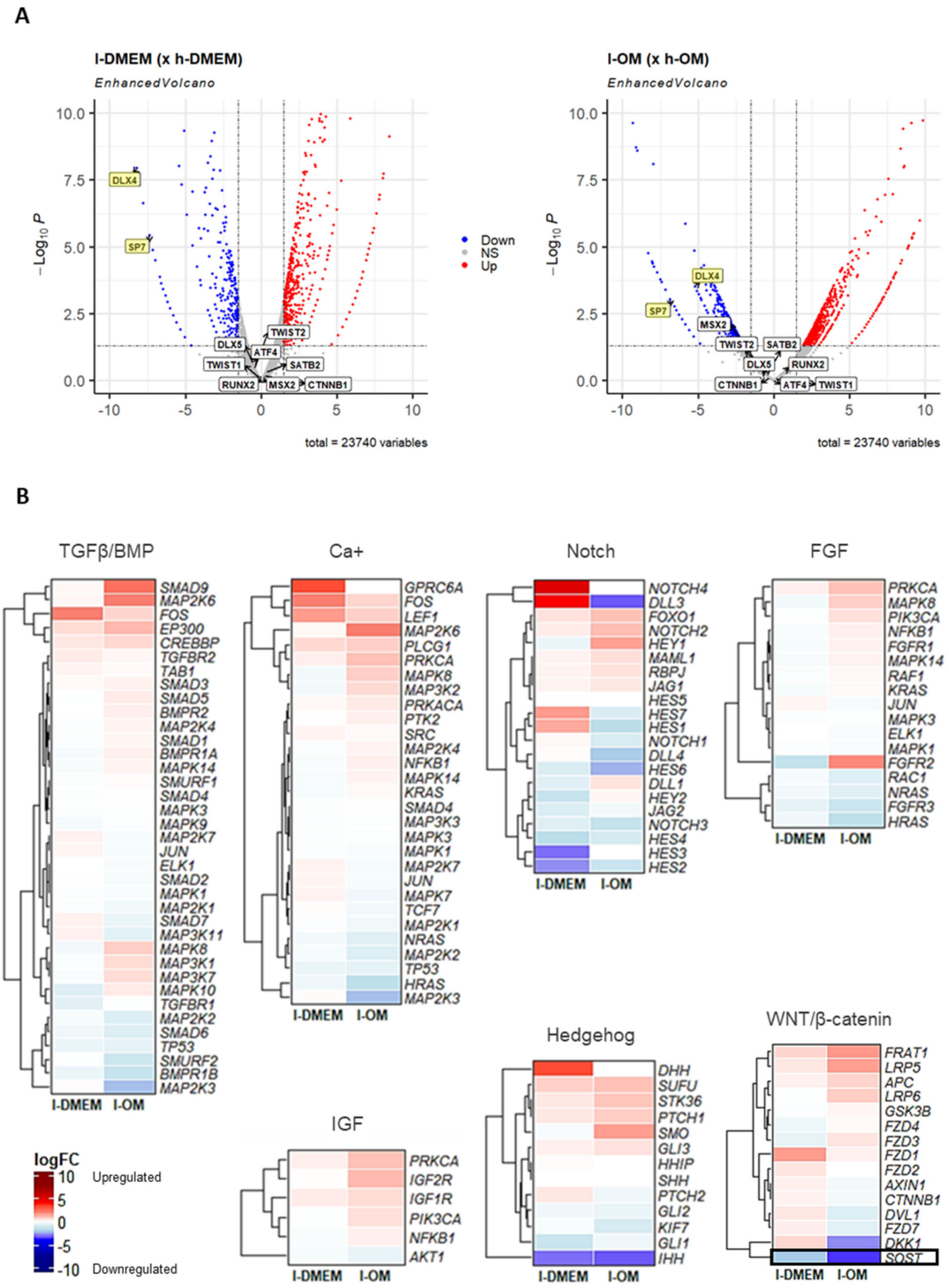


**Figure 3.** Analysis of other osteogenic TFs and signaling pathways in the RNA-seq dataset: The Volcano plots (**A**) show the magnitude of change in gene expression (logFC) and statistical significance (*p*-value) of the major osteogenic TFs, in l-DMEM (× h-DMEM) (left) and l-OM (× h-OM) (right). Highlighted in yellow are the *SP7* and *DLX4*, unique differentially expressed genes (logFC < −1.5 or >1.5 and *p*-value < 0.05) in both groups. Down: downregulated; Up: upregulated; NS: not significant. The Heatmap graphs (**B**) represent the logFC of the genes involved in the major osteogenic signaling pathways, in l-DMEM (× h-DMEM) and l-OM (× h-OM). It highlighted the *Sclerostin* (*SOST*) gene, a negative regulator of the WNT/β-catenin pathway, and was found to be differentially expressed (DEG) in both groups in l-PDLCs (× h-PDLCs). Reddish colors = upregulated; bluish colors = downregulated.

### *3.3. The lncRNAs LINC00939 and MIR31HG Are Upregulated in l-PDLCs*

The lncRNAs are important agents of the epigenetic machinery that act on the transcriptional, post-transcriptional, and translational regulations. Therefore, we also investigated the lncRNAs transcriptional profiles. Of all 1643 lncRNAs identified, 73 (≈4.5%) were DEGs (DElncRNAs) in the l-DMEM group and 82 (≈5%) in the l-OM group. There were 18 DElncRNAs in common among the groups, of which four long intergenic non-protein coding RNAs (*LINCs 00939*, *01260*, *01347* and *02210*), four uncharacterized (*LOCs 286178*, *408186*, *100506476* and *100507547*), and one host-gene (*MIR31HG*) were upregulated in both groups (Figure 4).

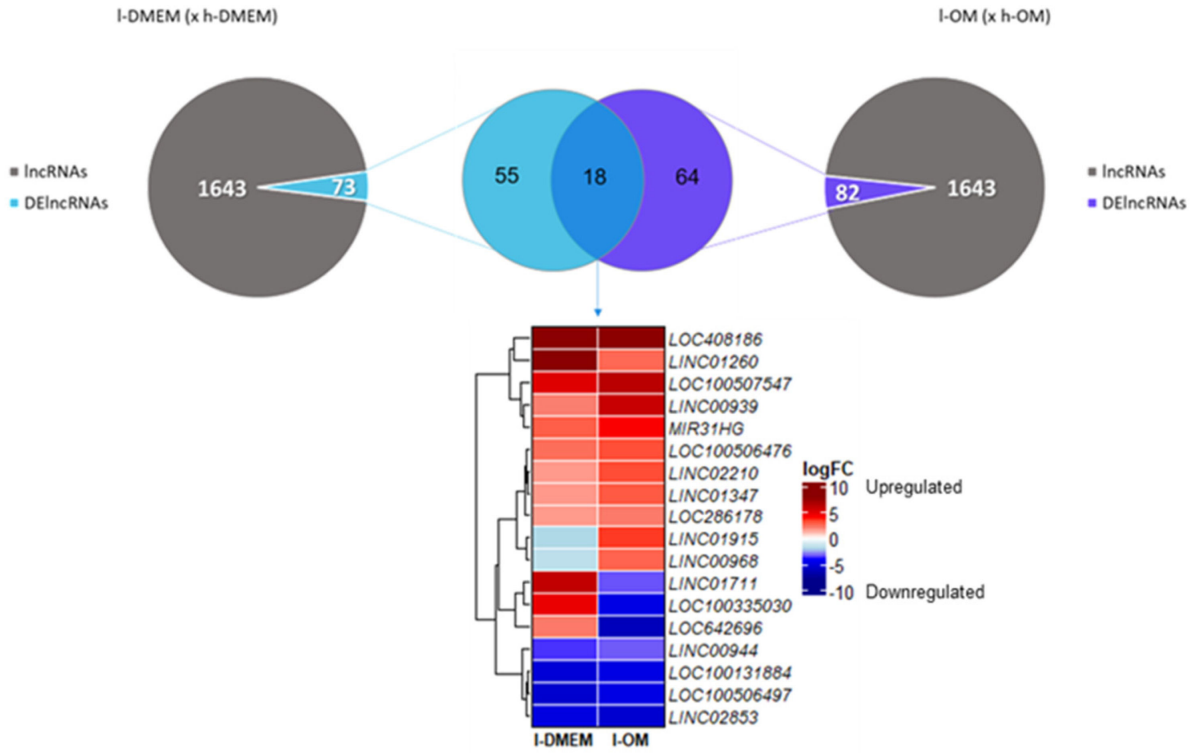


**Figure 4.** Analysis of lncRNAs in the RNA-seq dataset: The pie charts show the number of lncRNAs differentially expressed (DElncRNAs) in l-DMEM (x h-DMEM) (left) and l-OM (x h-OM) (right). The Venn diagram shows the number of DElncRNAs common and not common between the groups. The heatmap graph represents the logFC of the commons DElncRNAs, in both groups. Reddish colors = upregulated; bluish colors = downregulated.

### LncRNAs, MIR31HG and LINC00939 Are Predicted to Interact with SP7 and DLX4 by RNA:RNA Base-Pairing

The RNA:RNA base-pairing interaction is an epigenetic mechanism played by lncRNAs to regulate the genic post-transcription, in order to repress or promote the transcripts translation process. Aiming to verify the possibility of RNA:RNA base-pairing interaction between the TFs *SP7* and *DLX4*, and the DElncRNAs that are upregulated in common among l-DMEM and l-OM groups used the prediction program RIblast, based on the LncRRIsearch webserver. There were predicted interactions between SP7:MIR31HG, SP7:LINC00939 (Figure 5), DLX4:MIR31HG, and DLX4:LINC00939 (Figure 6). All interactions presented negative minimum energy (MinEnergy) <12 kcal/mol, which characterizes a high affinity of binding between the transcripts. Both MIR31HG and LINC00939 were identified as 3′ polyadenylated (Figure S1). The results corroborate the probability of post-transcriptional and/or translational repressive regulation on *SP7* and *DLX4* by MIR31HG and LINC00939 base-pairing interactions and suggest that these interactions occur passively, without the need for enzymes or catalytic molecular agents, due to the negative binding energy values presented.

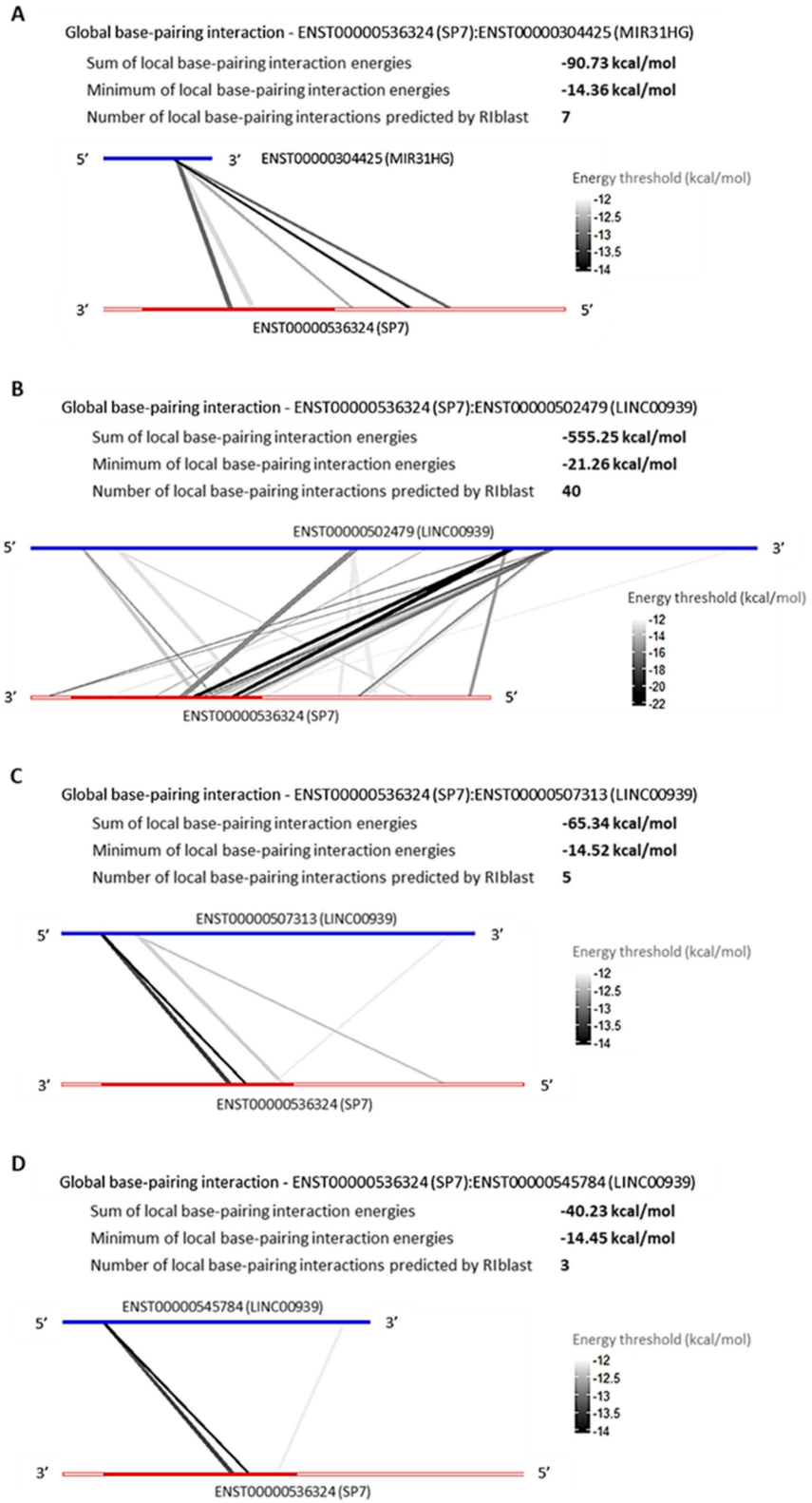


**Figure 5.** Global base-pairing interactions between SP7 and predicted DElncRNAs transcripts; Global base-pairing interactions between ENST00000536324 (SP7) and ENTS00000304425 (MIR31HG) (**A**), ENST00000502479 (LINC00939) (**B**), ENST00000507313 (LINC00939) (**C**), and ENST00000545784 (LINC00939) (**D**) transcripts. The blue bars represent the lncRNA transcripts and the red bars represent the SP7 transcript. The grayish lines represent the predicted interactions according to the energy threshold and SP7′s annotation (3′UTR, CDS, and 5′UTR regions).

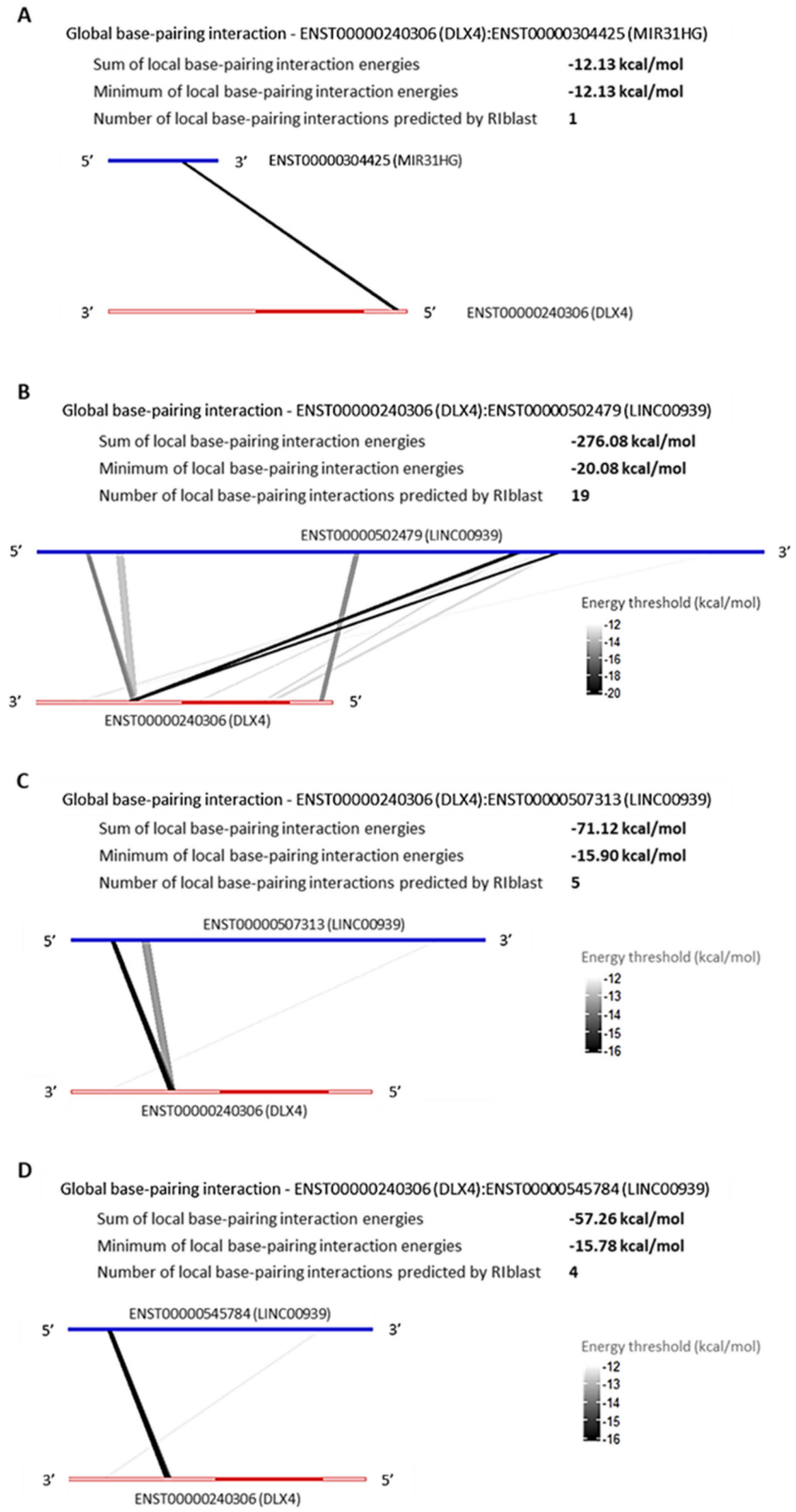


**Figure 6.** Global base-pairing interactions between DLX4 and predicted DElncRNAs transcripts; Global base-pairing interactions between ENST00000240306 (DLX4) and ENTS00000304425 (MIR31HG) (**A**), ENST00000502479 (LINC00939) (**B**), ENST00000507313 (LINC00939) (**C**), and ENST00000545784 (LINC00939) (**D**) transcripts. The blue bars represent the lncRNA transcripts and the red bars represent the DLX4 transcript. The grayish lines represent the predicted interactions according to the energy threshold and DLX4′s annotation (3′UTR, CDS, and 5′UTR regions).

### 3.4. Machine Learning Program Predicted Potential for DNA:RNA Triplex-Forming for the SP7 DNA Site and for the lncRNA LINC00939

Another epigenetic mechanism mediated by lncRNAs is the DNA:RNA triplex-forming, which consists of interactions between lncRNAs and DNA-specific sequences, via triple-helix (triplex) formation, to inhibit or induce gene transcriptions. We performed prediction analysis of DNA:RNA triplex-forming potential for the *SP7* and *DLX4* DNA sites and for the MIR31HG and LINC00939 transcripts. Triplex-forming potential was predicted for the *SP7* DNA sites (score = 0.68) (Table 1) and for the first exon (*ENSE00002048191*) of one LINC00939 transcript (*ENST00000502479.1*) (score = 0.75) (Table 2). Conversely, there was no prediction of triplex-forming potential for the *DLX4* DNA site, nor for the lncRNA MIR31HG. These results point to a potential transcriptional regulation on the *SP7* DNA site (inhibition) by triplex formation with the lncRNA LINC00939.

**Table 1.** Triplex prediction for the *SP7* and *DLX4* DNA sites.

| TRIPLEX DNA SITE PREDICTION | | | | | |
|---|---|---|---|---|---|
| **Gene Symbol** | **Assembly** | **Chromosome** | **Map Location** | **Score** | **Triplex-Forming** |
| SP7 | GRCh37 | 12 | 53720362:53739099 | 0.68235606 | Triplex |
| DLX4 | GRCh37 | 17 | 48046334:48052321 | 0.13426343 | Nontriplex |

### 3.5. MIR31HG and LINC00939 Transcripts Are Upregulated while SP7 and DLX4 Are Downregulated in l-PDLCs

In agreement with RNA-seq data, the expression of the lncRNAs, *MIR31HG* and *LINC00939*, were upregulated in l-PDLCs (× h-PDLCs) in both conditions, non-induced (DMEM) and induced (OM), with statistical significance for *MIR31HG* (l-DMEM × l-OM, $p = 0.001$; l-OM × h-OM, $p = 0.001$) and for *LINC00939* (l-DMEM × l-OM, $p = 0.004$; l-DMEM × h-DMEM, $p = 00.15$; l-OM × h-OM, $p < 0.0001$). In addition, the transcript levels of the osteogenic TFs *SP7* and *DLX4* in l-PDLCs were lower, with statistical significance for *SP7* (l-DMEM × l-OM, $p = 0.002$; l-DMEM × h-DMEM, $p < 0.0001$; h-DMEM × h-OM, $p = 0.004$; l-OM × h-OM, $p < 0.0001$), and for *DLX4* (h-DMEM × h-OM, $p = 0.005$; l-OM × h-OM, $p < 0.0002$) (Figure 7). These results show a negative correlation between *MIR31HG*/*LINC00939* and *SP7*/*DLX4* expression profiles, reinforcing the hypothesis of repressive action of these lncRNAs on the (post)transcriptional regulation of SP7 and DLX4.

**Table 2.** Triplex-forming potential of the lncRNAs MIR31HG and LINC00939.

| LNCRNAS TRIPLEX-FORMING POTENTIAL | | | | | |
|---|---|---|---|---|---|
| **Gene Symbol** | **Transcript ID** | **Annotation** | **Exon ID** | **Score** | **Triplex-Forming** |
| MIR31HG | ENST00000304425.3 | exon | ENSE00001540342 | 0.0 | Nontriplex |
| | | exon | ENSE00001540341 | 0.0 | Nontriplex |
| | | exon | ENSE00001540339 | 0.0 | Nontriplex |
| | | exon | ENSE00001729409 | 0.0 | Nontriplex |
| | | intron 1 | | 0.0 | Nontriplex |
| | | intron 2 | | 0.0 | Nontriplex |
| | | intron 3 | | 0.0 | Nontriplex |

**Table 2.** *Cont.*

| LNCRNAS TRIPLEX-FORMING POTENTIAL | | | | | |
|---|---|---|---|---|---|
| **Gene Symbol** | **Transcript ID** | **Annotation** | **Exon ID** | **Score** | **Triplex-Forming** |
| LINC00939 | ENST00000502479.1 | exon | ENSE00002048191 | 0.7498492 | Triplex |
| | | exon | ENSE00002044944 | 0.0 | Nontriplex |
| | | exon | ENSE00001441774 | 0.0 | Nontriplex |
| | | exon | ENSE00002049964 | 0.033063784 | Nontriplex |
| | | exon | ENSE00002021220 | 0.30899337 | Nontriplex |
| | | exon | ENSE00002063907 | 0.0 | Nontriplex |
| | | intron 1 | | 0.0 | Nontriplex |
| | | intron 2 | | 0.0 | Nontriplex |
| | | intron 3 | | 0.0 | Nontriplex |
| | | intron 4 | | 0.0 | Nontriplex |
| | | intron 5 | | 0.0 | Nontriplex |
| LINC00939 | ENST00000507313.1 | exon | ENSE00002060110 | 0.0 | Nontriplex |
| | | exon | ENSE00002044944 | 0.0 | Nontriplex |
| | | exon | ENSE00001441774 | 0.0 | Nontriplex |
| | | exon | ENSE00002033127 | 0.0 | Nontriplex |
| | | exon | ENSE00002081221 | 0.0 | Nontriplex |
| | | exon | ENSE00002046518 | 0.0 | Nontriplex |
| | | intron 1 | | 0.0 | Nontriplex |
| | | intron 2 | | 0.0 | Nontriplex |
| | | intron 3 | | 0.0 | Nontriplex |
| | | intron 4 | | 0.124810636 | Nontriplex |
| | | intron 5 | | 0.0 | Nontriplex |
| LINC00939 | ENST00000545784.1 | exon | ENSE00002206498 | 0.0 | Nontriplex |
| | | exon | ENSE00002044944 | 0.0 | Nontriplex |
| | | exon | ENSE00002228181 | 0.0 | Nontriplex |
| | | exon | ENSE00002271284 | 0.0 | Nontriplex |
| | | exon | ENSE00002021220 | 0.30899337 | Nontriplex |
| | | exon | ENSE00002216415 | 0.0 | Nontriplex |
| | | intron 1 | | 0.0 | Nontriplex |
| | | intron 2 | | 0.0 | Nontriplex |
| | | intron 3 | | 0.124810636 | Nontriplex |
| | | intron 4 | | 0.0 | Nontriplex |
| | | intron 5 | | 0.0 | Nontriplex |

Altogether, the results of chromatin accessibility, DNA methylation levels, RNA-seq, PCR, and predicted base-pairing interactions suggest *MIR31HG* and *LINC00939* might be good predictors of osteogenic commitment.

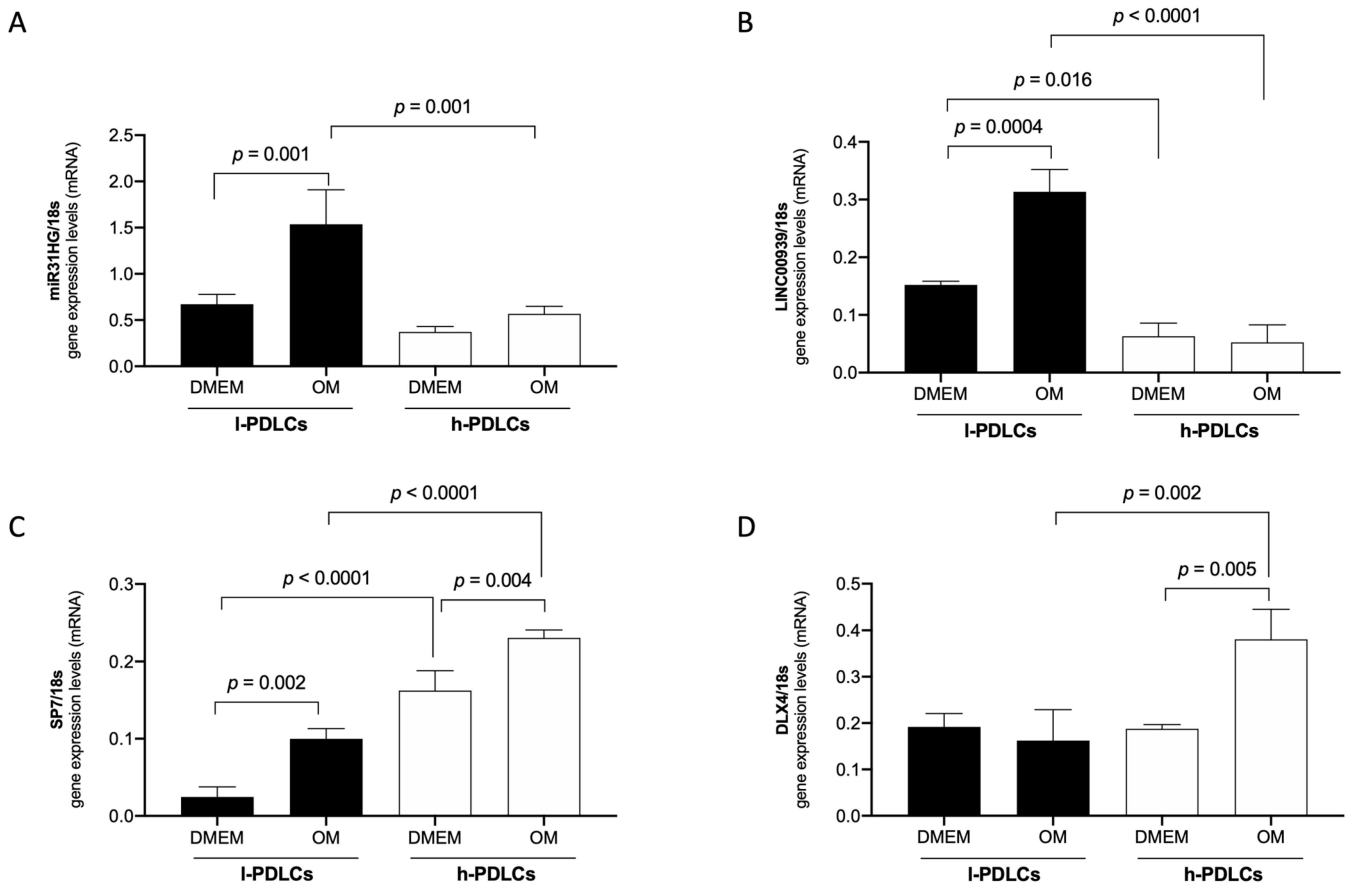


**Figure 7.** Gene expression levels of MIR31HG, LINC00939, SP7, and DLX4 in l- and h-PDLCs, cultured at 10 days in non-induced (DMEM) and osteogenic (OM) medium: qPCR analysis of MIR31HG (**A**), LINC00939 (**B**), SP7 (**C**), and DLX4 (**D**) in l- and h-PDLCs, cultured at 10 days in a non-induced (DMEM) and osteogenic (OM) medium. The results represent a mean ± standard deviation of three biological replicates, considering differential expression for $p < 0.05$.

## 4. Discussion

The advancement of genomic sequencing techniques and bioinformatic tools has helped us to better understand the epigenetic machinery involved in the phenotype acquisition of MSCs. Chromatin conformation, DNA methylation pattern, transcriptional profile, and ncRNAs interactions are part of this machinery and impact cell differentiation potential. Here, we aimed to investigate the epigenetic machinery of the transcription factors (TFs), *SP7* and *DLX4*, involved in the osteoblastic differentiation, in PDLCs, using omic techniques and bioinformatic tools. We provided data that indicate *SP7* and *DLX4* might be regulated at transcriptional, post-transcriptional, and translational steps by the epigenetic mediators MIR31HG and LINC00939 and this could impact their osteogenic phenotype acquisition. So far, our results indicate *MIR31HG* and *LINC00939* might be good predictors of osteogenic commitment.

In our previous investigation, we showed an epigenetic landscape more accessible in l-PDLCs, when compared to h-PDLCs [12]; however, several TFs such as *DLX4* and *SP7* were pointed out to be downregulated in l-PDLCs. Here, in the ATAC-seq analyses, we found more accessible chromatin peaks for both, *SP7* and *DLX4* genomic regions in l-PDLCs, when compared to h-PDLCs, except to the transcription end site (TES) region of the *DLX4*. One of the hypotheses for this discrepancy would be the differential presence, concentration, and action of some epigenetic chromatin regulators, such as DNA methyltransferases (DNMTs) and histone deacetylases (HDACs), among the PDLCs populations. Nevertheless, to verify this hypothesis, it would be necessary to integrate other analyses that were not performed

in this study, for example, chromatin immunoprecipitation (ChIP). The difference in peak score amplitude between l- and h-PDLCs was greater in *SP7* than in *DLX4*, and the peaks annotation also was distinct among the TFs genomic regions, with peaks concentration in exonic, TSS, and TES regions for *SP7*, and peaks concentration in intronic and TSS regions for *DLX4*. A study performed by Tai et al., in 2017, discovered a similar profile of chromatin accessibility on the *SP7* genomic region during the MC3T3 pre-osteoblast differentiation [42], with high chromatin accessibility centered within ~1 kb downstream of TES. Furthermore, this region coincided with CpG islands enrichments in *SP7*, indicating its importance in gene regulation. In the same, abovementioned study, accessible peaks were localized in the intronic region and in all osteoblastogenesis stages (pre-osteoblast, matrix deposition, nodule formation, and mineralization). These findings show chromatin conformation more favorable to *SP7* and *DLX4* transcription in l-PDLCs than h-PDLCs and suggest an important role of TES and intronic regions, i.e., non-promoter regions, on their gene regulations.

The TFs also presented distinct DNA methylation patterns to each other, without differentially methylated probes (DMPs) between l- and h-PDLCs. The average methylation intensities (AMIs) remained below 0.5 in all groups, indicating an overall DNA methylation pattern tending to unmethylated, except in the 3′UTR region of the *DLX4*, which presented AMIs above 0.5, ranged from 0.7 to 0.8, indicating DNA methylation pattern tending to totally methylated in this region. Conversely, very low methylation intensities were found in the 3′UTR region of the *SP7*, ranging around 0.03, which matches the high chromatin accessibility presented in ATAC-seq results for this TES region. In 2019, Lhoumaud et al. examined the interplay between chromatin accessibility and DNA methylation in mouse embryonic stem cells, using the *EpiMethylTag* method, that combined ATAC-seq with bisulfite conversion and showed that DNA methylation rarely coexists with chromatin accessibility [43].

The signaling pathways are complex cascades that are dependent on a "perfect syntony" among many molecular events to promote gene transcriptions. In our RNA-seq analyses, we did not find differentially expressed genes (DEGs) amongst l- and h-PDLCs in the main signaling pathways involved in the TFs gene transcription, except for the *Sclerostin* (*SOST*), which was found to be downregulated in l-PDLCs. Recent studies show a correlation of expression between *SOST* and several osteoblastic TFs, such as *RUNX2* and *SP7* [44,45]. This protein plays an important role in the osteoblast development, acting as an inhibitor of the Wnt/βcatenin pathway by binding to the cell transmembrane receptors low-density lipoprotein receptor protein 5 and 6 (LRP5/6) and Frizzled. However, the other genes of this pathway were not found in DEGs. Several studies show the repressor effect of Sirtuin 1 (SIRT1) on the *SOST* expression of osteocytes [46,47]. In our RNA-seq dataset, the *SIRT1* was found to be slightly upregulated in l-DMEM (logFC = 0.17) and l-OM (logFC = 0.49), without significant difference. So far, the results suggest a transcriptional status of the signaling pathways more favorable to TFs' expression in l-PDLCs compared to h-PDLCs.

Regarding the RNA-seq results for these TFs, our previous study [12] showed *SP7* and *DLX4* as DEGs and downregulated in both l-DMEM (x h-DMEM) and l-OM (x h-OM). However, these transcriptional profiles did not match the chromatin conformation or neither the DNA methylation pattern found here for these TFs. Both presented more accessible peaks, with higher peak scores in l-PDLCs than h-PDLCs, with DNA methylation patterns tending to be unmethylated in both populations. We expected to find opposite chromatin accessibility and DNA methylation patterns in l-PDLCs. Other studies also found discrepancies between ATAC-seq and RNA-seq results, and a positive correlation between DNA methylation and gene expression [48–50]. This paradox suggested the hypothesis of a fine-tuning gene regulation on *SP7* and *DLX4* in l-PDLCs, mediated by lncRNA interactions.

After we identified 18 lncRNAs DEGs in common between l-DMEM (x h-DMEM) and l-OM (x h-OM), only nine were upregulated in both groups, of which two (MIR31HG and LINC00939) were predicted by the web-based prediction tool to interact with *SP7* and *DLX4* by RNA:RNA base-pairing. This program is based on up-to-date benchmark data to compute the base-paring probabilities inter and intramolecular between RNA sequences [51].

The MIR31HG is a host gene of the MIR31, a miRNA validated as an SP7 repressor and osteogenesis inhibitor [52,53]. Nevertheless, to date, there are no studies correlating the *MIR31HG* and *SP7* expression profiles, nor predicting interactions between them. In 2018, Huang et al. cultivated BMSCs on titanium surfaces biofunctionalized with small interfering RNA (siRNA)-targeting MIR31HG and reported an increase in the relative expression of osteogenic genes such as *ALPL*, *RUNX2,* and *BGLAP*, without analyzing the *SP7* [54]. Since the MIR31HG hosts the MIR31, one possibility would be the MIR31HG produces precursors of MIR31 through intracellular shearing, and this represses the *SP7* [55]. However, the MIR31 was not found in DEG in our RNA-seq dataset, requiring a small RNA sequencing (miRNA-seq) to confirm this transcriptional profile. The LINC00939 is an Intergenic lncRNA, located on chromosome 12 (12q24.32), measuring 24,687 pairs of bases; although, we did not find previous publications about this lncRNA. Our hypothesis is both lncRNAs can regulate the post-transcriptional and/or translational processes of the *SP7* and *DLX4* by RNA:RNA base-pairing interactions. To the *SP7*, the interactions with MIR31HG were predicted in 5′UTR and coding sequence (CDS) regions, and LINC00939 was predicted with the majority being in the CDS region. In this case, both lncRNAs could repress the *SP7* post-transcription by "A to I" RNA edition, promoting hydrolytic deamination of adenosine to inosine [56], and/or the SP7 translation by the impediment of ribosome subunit binding. To the *DLX4*, the interaction with MIR31HG was predicted in the 5′UTR region, and LINC00939 predicted the majority in the 3′UTR region. In this case, the MIR31HG could repress the *DLX4* translation by the impediment of ribosome subunit binding, and the LINC00939 could repress the DLX4 post-transcription via Staufen-mediated decay, forming an intermolecular duplex with Alu element in the 3′UTR region [57,58]. Nonetheless, we should interpret these results with caution since the prediction tools "don't consider complex structure folding as RNA tertiary structures, non-canonical base-pairing and co-transcriptional folding process and may contain false-positive predictions" [35]. Thus, experimental validations involving silencing and/or overexpression of these lncRNAs followed by SP7 and DLX4 protein analyses are necessary to authenticate the causality of these predicted interactions.

Since RNA:RNA base-pairing is a post-transcriptional and translational regulatory mechanism, we also investigated the probability of transcriptional regulation by DNA:RNA triplex forming. For this purpose, we use the TriplexFPP, a machine learning program "based on the experimentally verified data, where the high-level features are learned by the convolutional neural networks" [37], which increases the potential of a triplex formation in practice. In contrast, the scarce number of validation assays limits the program training, which greatly restricts the scope of predictions. In our analysis, it was predicted a triplex target site (TTS) for the SP7 gene and triplex-forming oligonucleotide (TFO) for the exon *ENSE00002048191* of the LINC00939 transcript *ENST00000502479.1*. We hypothesize that the SP7:LINC00939 triplex-forming represses the *SP7* transcription by steric hindrance of the RNA polymerase II at the promoter region [20,59]. However, the program does not predict matching between TTS–TFO, requiring experimental assays, such as chromatin oligo-affinity precipitation (ChOP), to confirm this interaction [60,61].

Finally, in an attempt to identify markers to assist with the selection of PDLCs with distinct osteogenic potential, we selected a panel of four genes for further confirmation by qPCR. The panel included both lncRNAs, *MIR31HG* and *LINC0093,9* and both osteogenic TFs, *SP7* and *DLX4*. The confirmation and combination of higher levels of *MIR31HG* and *LINC00939* transcripts alongside lower levels of *SP7* and *DLX4* gene expression in l-PDLCs after in vitro osteogenic induction indeed show potential in predicting distinct osteogenic

potential amongst PDLCs. Surprisingly, there was no correlation between qPCR and RNA-seq results for the *DLX4* gene expression among the l- and h-DMEM. Everaert et al. also reported discrepancies among qPCR and RNA-seq gene expression measurements, typically in smaller genes [62]. Coincidentally, *DLX4* was the smallest gene analyzed here (sizes: *DLX4* ≈ 6 kb; SP7 ≈ 18 kb; LINC00939 ≈ 24 kb; MIR31HG ≈ 104 kb).

Further studies with functional approach by silencing and overexpressing the lncRNAs, *MIR31HG* and *LINC00939,* and the impact on *SP7* and *DLX4* gene expression will be necessary to confirm the hypothesis here identified.

## 5. Conclusions

The set of results obtained here indicates the lncRNAs, MIR31HG and LINC00939, as possible epigenetic mediators on PDLCs osteogenic phenotype commitment through repressive regulation of the osteogenic TFs, *SP7* and *DLX4* (Figure 8). In this regard, *MIR31HG* and *LINC00939* might be good predictors of osteogenic commitment in PDLCs.

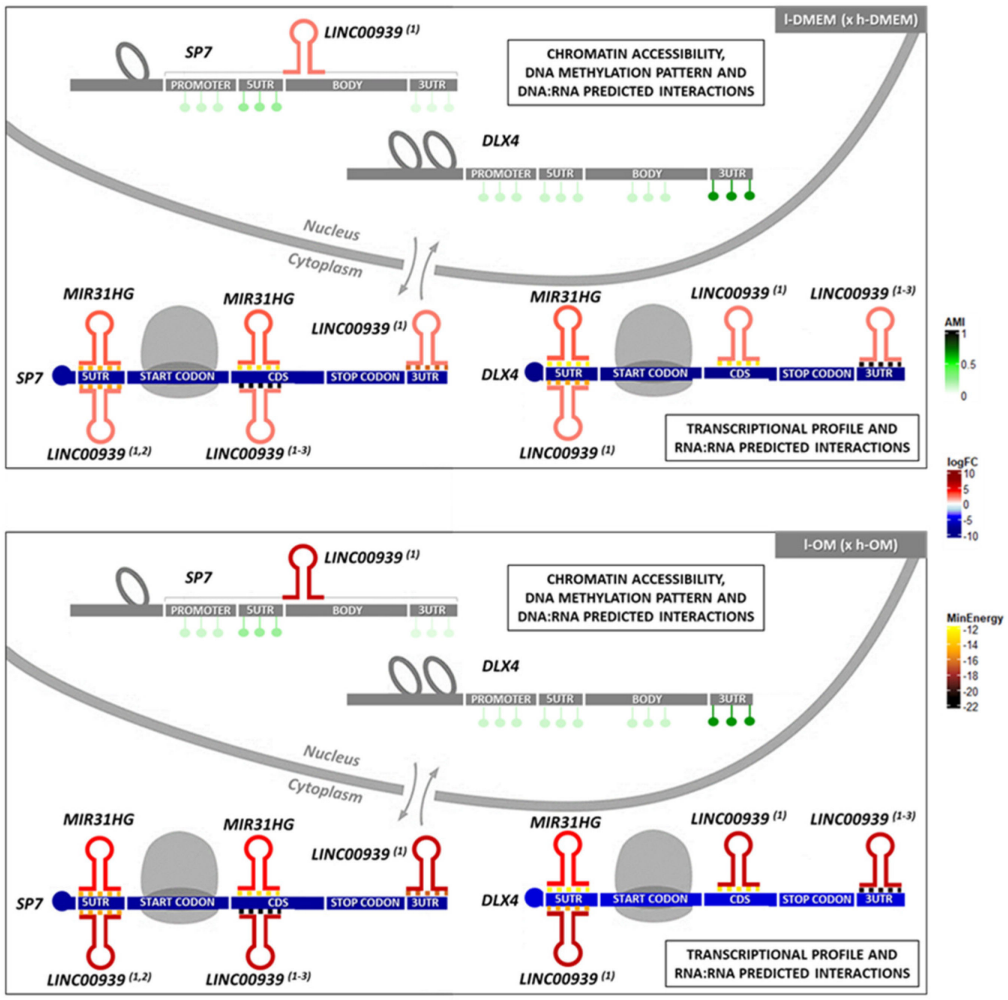


**Figure 8.** Schematic representation of the SP7 and DLX4 epigenetic status and their predicted interactions with the lncRNAs, MIR31HG and LINC00939, in l-PDLCs (× h-PDLCs) at 10 days, cultured in DMEM and OM medium: The results of the ATAC-seq dataset show the chromatin is more accessible for the SP7 and DLX4 genes in l-PDLCs (DMEM and OM) compared with h-PDLCs (DMEM and OM). The results of the Methylome dataset show a less methylated pattern for the SP7 and DLX4 genes, in all groups, except to the 3′UTR region of the DLX4, which exhibit a more methylated pattern. The lncRNAs analyses in the RNA-seq dataset show the DElncRNAs MIR31HG and LINC00939 (predicted to interact with SP7 and DLX4 by RNA:RNA base-pairing) upregulated in

both l-DMEM (× h-DMEM) and l-OM (× h-OM) groups. The DNA:RNA interactions analyses predicted potential triplex-forming for one LINC00939 transcript (ENST00000502479) and for the SP7 DNA site, in practice. These data together allow us to hypothesize the existence of a possible transcriptional repressor regulation on the SP7 by triplex-forming with LINC00939, and a post-transcriptional repressor regulation on the SP7 and DLX4 transcripts by MIR31HG and LINC00939 base-pairing interactions, in l-PDLCs at 10 days, cultured in DMEM and OM medium. (1) = ENST00000502479; (2) = ENST00000507313; (3) = ENST00000545784; CDS = coding DNA sequence; reddish colors = upregulated; bluish colors = downregulated; greenish colors = average methylation intensity (AMI); yellowish and brownish colors = minimum energy (kcal/mol) of the predicted RNA:RNA interactions. Adapted from Gomes et al., 2020 [63].

**Supplementary Materials:** The following supporting information can be downloaded at: https://www.mdpi.com/article/10.3390/genes14081649/s1, Table S1. Gene expression primers sequences and polymerase chain reaction cycle conditions. Figure S1. Search results for poly(A) sites on the genomic regions of the MIR31HG and LINC00939 lncRNAs.

**Author Contributions:** Conceptualization, R.S.F., R.A.d.S., M.W. and D.C.A.; methodology, R.S.F. and R.I.F.A.; validation, R.S.F., R.I.F.A. and F.R., formal analysis, R.S.F., F.R. and A.C.B.; investigation, R.S.F., R.I.F.A., F.R. and A.C.B.; resources, R.A.d.S., M.W. and D.C.A.; data curation, R.S.F.; writing—original draft preparation, R.S.F.; writing—review and editing, R.S.F., R.I.F.A., F.R., A.C.B., R.A.d.S., M.W. and D.C.A.; visualization, R.S.F. and D.C.A.; supervision, D.C.A.; project administration, D.C.A.; funding acquisition, R.S.F., M.W. and D.C.A. All authors have read and agreed to the published version of the manuscript.

**Funding:** This research was funded by São Paulo Research Foundation-FAPESP/The University of Birmingham, UK Collaborative Research Program (grant number 2017/07944-5) and The APC was funded by Paulista University.

**Institutional Review Board Statement:** The study was conducted in accordance with the Declaration of Helsinki and approved by the Ethics Committee of Piracicaba Dental School, University of Campinas, São Paulo, Brazil (CAAE55588816.4.0000.5418).

**Informed Consent Statement:** Written informed consent has been obtained from the patient(s) to publish this paper.

**Data Availability Statement:** The data presented in this study are available on request from the corresponding authors. The data are not publicly available due to potentially identifiable genomic information.

**Conflicts of Interest:** The authors declare no conflict of interest.

## References

1. Hmadcha, A.; Martin-Montalvo, A.; Gauthier, B.R.; Soria, B.; Capilla-Gonzalez, V. Therapeutic potential of mesenchymal stem cells for cancer therapy. *Front. Bioeng. Biotechnol.* **2020**, *8*, 43. [CrossRef] [PubMed]
2. Meirelles, L.D.S.; Chagastelles, P.C.; Nardi, N.B. Mesenchymal stem cells reside in virtually all post-natal organs and tissues. *J. Cell. Sci.* **2006**, *119*, 2204–2213. [CrossRef] [PubMed]
3. Hargreaves, K.M.; Diogenes, A.; Teixeira, F.B. Treatment options: Biological basis of regenerative endodontic procedures. *Pediatr. Dent.* **2013**, *35*, 129–140. [CrossRef]
4. Dominici, M.L.B.K.; Le Blanc, K.; Mueller, I.; Slaper-Cortenbach, I.; Marini, F.C.; Krause, D.S.; Deans, R.J.; Keating, A.; Prockop, D.J.; Horwitz, E.M. Minimal criteria for defining multipotent mesenchymal stromal cells: The International Society for Cellular Therapy position statement. *Cytotherapy* **2006**, *8*, 315–317. [CrossRef] [PubMed]
5. Salgado, A.J.; Reis, R.L.; Sousa, N.; Gimble, J.M. Adipose tissue derived stem cells secretome: Soluble factors and their roles in regenerative medicine. *Curr. Stem Cell Res. Ther.* **2010**, *5*, 103–110. [CrossRef]
6. Jiang, Y.; Jahagirdar, B.N.; Reinhardt, R.L.; Schwartz, R.E.; Keene, C.D.; Ortiz-Gonzalez, X.R.; Reyes, M.; Lenvik, T.; Lund, T.; Blackstad, M.; et al. Pluripotency of mesenchymal stem cells derived from adult marrow. *Nature* **2002**, *418*, 41–49. [CrossRef]
7. Sevari, S.P.; Ansari, S.; Moshaverinia, A. A narrative overview of utilizing biomaterials to recapitulate the salient regenerative features of dental-derived mesenchymal stem cells. *Int. J. Oral Sci.* **2021**, *13*, 22. [CrossRef]
8. Saito, M.T.; Salmon, C.R.; Amorim, B.R.; Ambrosano, G.M.; Casati, M.Z.; Sallum, E.A.; Nociti, F.H., Jr.; Silvério, K.G. Characterization of highly osteoblast/cementoblast cell clones from a CD105-enriched periodontal ligament progenitor cell population. *J. Periodontol.* **2014**, *85*, e205–e211. [CrossRef]

9. Assis, R.I.; Feltran, G.D.S.; Silva, M.E.S.; do Rosário Palma, I.C.; Rovai, E.S.; de Miranda, T.B.; Ferreira, M.R.; Zambuzzi, W.F.; Birbrair, A.; Andia, D.C.; et al. Non-coding RNAs repressive role in post-transcriptional processing of RUNX2 during the acquisition of the osteogenic phenotype of periodontal ligament mesenchymal stem cells. *Dev. Biol.* **2021**, *470*, 37–48. [CrossRef]
10. Assis, R.I.; Schmidt, A.G.; Racca, F.; da Silva, R.A.; Zambuzzi, W.F.; Silvério, K.G.; Nociti, F.H., Jr.; Pecorari, V.G.; Wiench, M.; Andia, D.C. DNMT1 inhibitor restores RUNX2 expression and mineralization in periodontal ligament cells. *DNA Cell Biol.* **2021**, *40*, 662–674. [CrossRef]
11. Ferreira, R.S.; Assis, R.I.; Feltran, G.D.S.; do Rosário Palma, I.C.; Françoso, B.G.; Zambuzzi, W.F.; Andia, D.C.; da Silva, R.A. Genome-wide DNA (hydroxy) methylation reveals the individual epigenetic landscape importance on osteogenic phenotype acquisition in periodontal ligament cells. *J. Periodontol.* **2022**, *93*, 435–448. [CrossRef] [PubMed]
12. Assis, R.I.; Racca, F.; Ferreira, R.S.; Ruiz, K.G.; da Silva, R.A.; Clokie, S.J.; Wiench, M.; Andia, D.C. Osteogenic commitment of human periodontal ligament cells is predetermined by methylation, chromatin accessibility and expression of key transcription factors. *Cells* **2022**, *11*, 1126. [CrossRef] [PubMed]
13. Stein, G.S.; Zaidi, S.K.; Stein, J.L.; Lian, J.B.; Van Wijnen, A.J.; Montecino, M.; Young, D.W.; Javed, A.; Pratap, J.; Choi, J.; et al. Transcription-factor-mediated epigenetic control of cell fate and lineage commitment. *Biochem. Cell Biol.* **2009**, *87*, 1–6. [CrossRef] [PubMed]
14. Morrison, O.; Thakur, J. Molecular complexes at euchromatin, heterochromatin and centromeric chromatin. *Int. J. Mol. Sci.* **2021**, *22*, 6922. [CrossRef]
15. Bird, A. DNA methylation patterns and epigenetic memory. *Genes Dev.* **2002**, *16*, 6–21. [CrossRef]
16. Lambert, S.A.; Jolma, A.; Campitelli, L.F.; Das, P.K.; Yin, Y.; Albu, M.; Chen, X.; Taipale, J.; Hughes, T.R.; Weirauch, M.T. The human transcription factors. *Cell* **2018**, *172*, 650–665. [CrossRef]
17. Pratt, A.J.; MacRae, I.J. The RNA-induced silencing complex: A versatile gene-silencing machine. *J. Biol. Chem.* **2009**, *284*, 17897–17901. [CrossRef]
18. Kunkler, C.N.; Hulewicz, J.P.; Hickman, S.C.; Wang, M.C.; McCown, P.J.; Brown, J.A. Stability of an RNA• DNA–DNA triple helix depends on base triplet composition and length of the RNA third strand. *Nucleic Acids Res.* **2019**, *47*, 7213–7222. [CrossRef]
19. Li, Y.; Syed, J.; Sugiyama, H. RNA-DNA triplex formation by long noncoding RNAs. *Cell Chem. Biol.* **2016**, *23*, 1325–1333. [CrossRef]
20. Statello, L.; Guo, C.J.; Chen, L.L.; Huarte, M. Gene regulation by long non-coding RNAs and its biological functions. *Nat. Rev. Mol. Cell Biol.* **2021**, *22*, 96–118. [CrossRef]
21. Silvério, K.G.; Rodrigues, T.L.; Coletta, R.D.; Benevides, L.; Da Silva, J.S.; Casati, M.Z.; Sallum, E.A.; Nociti, F.H., Jr. Mesenchymal stem cell properties of periodontal ligament cells from deciduous and permanent teeth. *J. Periodontol.* **2010**, *81*, 1207–1215. [CrossRef] [PubMed]
22. UCSC: Genome Browser. University of California Santa Cruz. Available online: https://genome.ucsc.edu/ (accessed on 28 May 2023).
23. Buenrostro, J.D.; Wu, B.; Chang, H.Y.; Greenleaf, W.J. ATAC-seq: A method for assaying chromatin accessibility genome-wide. *Curr. Protoc. Mol. Biol.* **2015**, *109*, 21–29. [CrossRef]
24. Corces, M.R.; Buenrostro, J.D.; Wu, B.; Greenside, P.G.; Chan, S.M.; Koenig, J.L.; Snyder, M.P.; Pritchard, J.K.; Kundaje, A.; Greenleaf, W.J.; et al. Lineage-specific and single-cell chromatin accessibility charts human hematopoiesis and leukemia evolution. *Nat. Genet.* **2016**, *48*, 1193–1203. [CrossRef] [PubMed]
25. Langmead, B.; Salzberg, S.L. Fast gapped-read alignment with Bowtie 2. *Nat. Methods* **2012**, *9*, 357–359. [CrossRef] [PubMed]
26. Heinz, S.; Benner, C.; Spann, N.; Bertolino, E.; Lin, Y.C.; Laslo, P.; Cheng, J.X.; Murre, C.; Singh, H.; Glass, C.K. Simple combinations of lineage-determining transcription factors prime cis-regulatory elements required for macrophage and B cell identities. *Mol. Cell* **2010**, *38*, 576–589. [CrossRef]
27. Illumina: GenomeStudio Software. Available online: https://www.illumina.com/techniques/microarrays/array-data-analysis-experimental-design/genomestudio.html (accessed on 28 May 2023).
28. Aryee, M.J.; Jaffe, A.E.; Corrada-Bravo, H.; Ladd-Acosta, C.; Feinberg, A.P.; Hansen, K.D.; Irizarry, R.A. Minfi: A flexible and comprehensive Bioconductor package for the analysis of Infinium DNA methylation microarrays. *Bioinformatics* **2014**, *30*, 1363–1369. [CrossRef]
29. Wickham, H.; François, R.; Henry, L.; Müller, K. dplyr: A Grammar of Data Manipulation. Available online: https://github.com/tidyverse/dplyr (accessed on 28 May 2023).
30. Wickham, H.; Averick, M.; Bryan, J.; Chang, W.; McGowan, L.D.A.; François, R.; Grolemund, G.; Hayes, A.; Henry, L.; Hester, J.; et al. Welcome to the Tidyverse. *J. Open Source Softw.* **2019**, *4*, 1686. [CrossRef]
31. Liao, Y.; Smyth, G.K.; Shi, W. The R package Rsubread is easier, faster, cheaper and better for alignment and quantification of RNA sequencing reads. *Nucleic Acids Res.* **2019**, *47*, e47. [CrossRef]
32. Robinson, M.D.; McCarthy, D.J.; Smyth, G.K. edgeR: A Bioconductor package for differential expression analysis of digital gene expression data. *Bioinformatics* **2010**, *26*, 139–140. [CrossRef]
33. Gu, Z.; Eils, R.; Schlesner, M. Complex heatmaps reveal patterns and correlations in multidimensional genomic data. *Bioinformatics* **2016**, *32*, 2847–2849. [CrossRef]
34. Blighe, K.; Rana, S.; Lewis, M. EnhancedVolcano: Publication-ready volcano plots with enhanced coloring and labeling. In *R Package Version 1.8.0*; R Foundation for Statistical Computing: Vienna, Austria, 2020.

35. Fukunaga, T.; Iwakiri, J.; Ono, Y.; Hamada, M. LncRRIsearch: A web server for lncRNA-RNA interaction prediction integrated with tissue-specific expression and subcellular localization data. *Front. Genet.* **2019**, *10*, 462. [CrossRef] [PubMed]
36. Herrmann, C.J.; Schmidt, R.; Kanitz, A.; Artimo, P.; Gruber, A.J.; Zavolan, M. PolyASite 2.0: A consolidated atlas of polyadenylation sites from 3′ end sequencing. *Nucleic Acids Res.* **2020**, *48*, D174–D179. [CrossRef] [PubMed]
37. Zhang, Y.; Long, Y.; Kwoh, C.K. Deep learning based DNA: RNA triplex forming potential prediction. *BMC Bioinform.* **2020**, *21*, 522. [CrossRef]
38. Cunningham, F.; Allen, J.E.; Allen, J.; Alvarez-Jarreta, J.; Amode, M.R.; Armean, I.M.; Austine-Orimoloye, O.; Azov, A.G.; Barnes, I.; Bennett, R.; et al. Ensembl 2022. *Nucleic Acids Res.* **2022**, *50*, D988–D995. [CrossRef] [PubMed]
39. Heberle, H.; Meirelles, G.V.; da Silva, F.R.; Telles, G.P.; Minghim, R. InteractiVenn: A web-based tool for the analysis of sets through Venn diagrams. *BMC Bioinform.* **2015**, *16*, 169. [CrossRef]
40. Assis, R.I.; Wiench, M.; Silverio, K.G.; da Silva, R.A.; Feltran, G.D.S.; Sallum, E.A.; Casati, M.Z.; Nociti, F.H., Jr.; Andia, D.C. RG108 increases NANOG and OCT4 in bone marrow-derived mesenchymal cells through global changes in DNA modifications and epigenetic activation. *PLoS ONE* **2018**, *13*, e0207873. [CrossRef] [PubMed]
41. Schmittgen, T.D.; Livak, K.J. Analyzing real-time PCR data by the comparative CT method. *Nat. Protoc.* **2008**, *3*, 1101–1108. [CrossRef]
42. Tai, P.W.; Wu, H.; Van Wijnen, A.J.; Stein, G.S.; Stein, J.L.; Lian, J.B. Genome-wide DNase hypersensitivity, and occupancy of RUNX2 and CTCF reveal a highly dynamic gene regulome during MC3T3 pre-osteoblast differentiation. *PLoS ONE* **2017**, *12*, e0188056. [CrossRef]
43. Lhoumaud, P.; Sethia, G.; Izzo, F.; Sakellaropoulos, T.; Snetkova, V.; Vidal, S.; Badri, S.; Cornwell, M.; Giammartino, D.C.D.G.; Kim, K.T.; et al. EpiMethylTag: Simultaneous detection of ATAC-seq or ChIP-seq signals with DNA methylation. *Genome Biol.* **2019**, *20*, 248. [CrossRef]
44. Pérez-Campo, F.M.; Santurtún, A.; García-Ibarbia, C.; Pascual, M.A.; Valero, C.; Garcés, C.; Sañudo, C.; Zarrabeitia, M.T.; Riancho, J.A. Osterix and RUNX2 are transcriptional regulators of sclerostin in human bone. *Calcif. Tissue Int.* **2016**, *99*, 302–309. [CrossRef]
45. Ohyama, Y.; Nifuji, A.; Maeda, Y.; Amagasa, T.; Noda, M. Spaciotemporal association and bone morphogenetic protein regulation of sclerostin and osterix expression during embryonic osteogenesis. *Endocrinology* **2004**, *145*, 4685–4692. [CrossRef] [PubMed]
46. Cohen-Kfir, E.; Artsi, H.; Levin, A.; Abramowitz, E.; Bajayo, A.; Gurt, I.; Zhong, L.; D'Urso, A.; Toiber, D.; Mostoslavsky, R.; et al. Sirt1 is a regulator of bone mass and a repressor of Sost encoding for sclerostin, a bone formation inhibitor. *Endocrinology* **2011**, *152*, 4514–4524. [CrossRef] [PubMed]
47. Kim, J.M.; Yang, Y.S.; Xie, J.; Lee, O.; Kim, J.; Hong, J.; Boldyreff, B.; Filhol, O.; Chun, H.; Greenblatt, M.B.; et al. Regulation of sclerostin by the SIRT1 stabilization pathway in osteocytes. *Cell Death Differ.* **2022**, *29*, 1625–1638. [CrossRef] [PubMed]
48. Starks, R.R.; Biswas, A.; Jain, A.; Tuteja, G. Combined analysis of dissimilar promoter accessibility and gene expression profiles identifies tissue-specific genes and actively repressed networks. *Epigenetics Chromatin* **2019**, *12*, 16. [CrossRef]
49. Anastasiadi, D.; Esteve-Codina, A.; Piferrer, F. Consistent inverse correlation between DNA methylation of the first intron and gene expression across tissues and species. *Epigenetics Chromatin* **2018**, *11*, 37. [CrossRef]
50. Wang, K.; Dai, R.; Xia, Y.; Tian, J.; Jiao, C.; Mikhailova, T.; Zhang, C.; Chen, C.; Liu, C. Spatiotemporal specificity of correlated DNA methylation and gene expression pairs across different human tissues and stages of brain development. *Epigenetics* **2022**, *17*, 1110–1127. [CrossRef]
51. Fukunaga, T.; Hamada, M. RIblast: An ultrafast RNA–RNA interaction prediction system based on a seed-and-extension approach. *Bioinformatics* **2017**, *33*, 2666–2674. [CrossRef]
52. Baglìo, S.R.; Devescovi, V.; Granchi, D.; Baldini, N. MicroRNA expression profiling of human bone marrow mesenchymal stem cells during osteogenic differentiation reveals Osterix regulation by miR-31. *Gene* **2013**, *527*, 321–331. [CrossRef]
53. McCully, M.; Conde, J.; Baptista, P.V.; Mullin, M.; Dalby, M.J.; Berry, C.C. Nanoparticle-antagomiR based targeting of miR-31 to induce osterix and osteocalcin expression in mesenchymal stem cells. *PLoS ONE* **2018**, *13*, e0192562. [CrossRef]
54. Huang, Y.; Zheng, Y.; Xu, Y.; Li, X.; Zheng, Y.; Jia, L.; Li, W. Titanium surfaces functionalized with siMIR31HG promote osteogenic differentiation of bone marrow mesenchymal stem cells. *ACS Biomater. Sci. Eng.* **2018**, *4*, 2986–2993. [CrossRef]
55. Zhang, X.; Wang, W.; Zhu, W.; Dong, J.; Cheng, Y.; Yin, Z.; Shen, F. Mechanisms and functions of long non-coding RNAs at multiple regulatory levels. *Int. J. Mol. Sci.* **2019**, *20*, 5573. [CrossRef] [PubMed]
56. Slotkin, W.; Nishikura, K. Adenosine-to-inosine RNA editing and human disease. *Genome Med.* **2013**, *5*, 105. [CrossRef] [PubMed]
57. Gong, C.; Maquat, L.E. lncRNAs transactivate STAU1-mediated mRNA decay by duplexing with 3′ UTRs via Alu elements. *Nature* **2011**, *470*, 284–288. [CrossRef]
58. Park, E.; Maquat, L.E. Staufen-mediated mRNA decay. *Wiley Interdiscip. Rev. RNA* **2013**, *4*, 423–435. [CrossRef] [PubMed]
59. Browning, D.F.; Busby, S.J. The regulation of bacterial transcription initiation. *Nat. Rev. Microbiol.* **2004**, *2*, 57–65. [CrossRef]
60. Mondal, T.; Subhash, S.; Vaid, R.; Enroth, S.; Uday, S.; Reinius, B.; Mitra, S.; Mohammed, A.; James, A.R.; Hoberg, E.; et al. MEG3 long noncoding RNA regulates the TGF-β pathway genes through formation of RNA–DNA triplex structures. *Nat. Commun.* **2015**, *6*, 7743. [CrossRef] [PubMed]
61. Rossi, M.N.; Maione, R. Identification of chromatin binding sites for long noncoding RNAs by chromatin oligo-affinity precipitation (ChOP). In *RNA-Chromatin Interactions: Methods and Protocols*; Humana: New York, NY, USA, 2020; pp. 17–28. ISBN 978-1-0716-0680-3.

62. Everaert, C.; Luypaert, M.; Maag, J.L.; Cheng, Q.X.; Dinger, M.E.; Hellemans, J.; Mestdagh, P. Benchmarking of RNA-sequencing analysis workflows using whole-transcriptome RT-qPCR expression data. *Sci. Rep.* **2017**, *7*, 1559. [CrossRef] [PubMed]
63. Gomes, C.P.D.C.; Schroen, B.; Kuster, G.M.; Robinson, E.L.; Ford, K.; Squire, I.B.; Heymans, S.; Martelli, F.; Emanueli, C.; Devaux, Y.; et al. Regulatory RNAs in heart failure. *Circulation* **2020**, *141*, 313–328. [CrossRef]

## 3. ARTIGO 2 (SUBMETIDO À REVISTA *ORAL DISEASES*)

# JARID1B represses the osteogenic potential of human periodontal ligament mesenchymal cells.

**Running Title:** JARID1B represses the osteogenic phenotype in PDLCs.

**Keywords:** Bone; Epigenetics; Mesenchymal Stem Cells; JARID1B; PDLC, Osteoblast.

Rogério S. Ferreira[*]; Rodrigo A. da Silva[† ‡]; Geórgia da S. Feltran[‡], Ericka Patricia da Silva[†]; Rahyza I F de Assis[§]; Emanuel Silva Rovai[‖]; Willian F. Zambuzzi[‡]; Denise C. Andia[*]

The authors R.S.F. and R.A.S. contributed equally to this study.

*Corresponding author:*

Denise Carleto Andia

School of Dentistry, Health Science Institute, Paulista University

Dr. Bacelar St., 1212, São Paulo, SP, 04026-002, Brazil.

Email: denise.andia@docente.unip.br

Phone: +55 (11) 5594 3207

Submitted on 23 June 2023

Revised on 15 August 2023

Resubmitted on 06 September 2023

[*] School of Dentistry, Health Science Institute, Paulista University, São Paulo, Brazil.
[†] CEEpiRG, Program in Environmental and Experimental Pathology, Paulista University – UNIP, São Paulo, São Paulo, Brazil.
[‡] Lab. of Bioassays and Cellular Dynamics, Department of Chemistry and Biochemistry, Institute of Biosciences, UNESP – São Paulo State University, Botucatu, São Paulo, Brazil.
[§] Department of Clinical Dentistry, Federal University of Espírito Santo, Vitória, ES, Brazil.
[‖] Division of Periodontics, Unesp - São Paulo State University, Institute of Science and Technology, São José dos Campos, São Paulo, Brazil.

## ABSTRACT

**Background:** Here, we evaluated whether the histone lysine demethylase 5B (JARID1B), is involved in osteogenic phenotype commitment of periodontal ligament cells (PDLCs), by considering their heterogeneity for osteoblast differentiation.

**Materials and Methods:** Epigenetic, transcriptional and protein levels of a gene set, involved in the osteogenesis, were investigated by performing genome-wide DNA (hydroxy)methylation, mRNA expression and western blotting analysis at basal (without osteogenic induction), and at the 3rd and 10th days of osteogenic stimulus, *in vitro,* using PDLCs with low (l) and high (h) osteogenic potential as biological models.

**Results:** h-PDLCs showed reduced levels of *JARID1B*, compared to l-PDLCs, with significant inversely proportional correlations between *RUNX2* and *RUNX2/p57*. Epigenetically, a significant reduction in the global H3K4me3 content was observed only in h-PDLCs. Immunoblotting data reveals a significant reduction in the global H3K4me3 content, at 3 days of induction only in h-PDLCs, while an increase in the global H3K4me3 content was observed at 10 days for both PDLCs. Additionally, positive correlations were found between global H3K4me3 levels and *JARID1B* gene expression.

**Conclusions:** Altogether, our results show the crucial role of JARID1B in repressing PDLCs osteogenic phenotype and this claims to pre-clinical protocols proposing JARID1B as a potential therapeutic target.

## INTRODUCTION

Bone repair and healing are major events in periodontal regeneration requiring a well-defined sequential activation of molecular and signaling mechanisms, with a well-coordinated set of actions among different signaling pathways grouped in several steps, following a determined timeline sequence (Rux et al., 2017; Cho, Gerstenfeld & Einhorn, 2002). These advances in our knowledge have been proposed in bone bioengineering and guiding researchers on looking for the ideal biomaterial (Baroncelli et al., 2019). Mechanistically, bone healing requires the recruitment and further proper differentiation of mesenchymal stem cells (MSC), promoting an adequate tissue repairment, by preserving the tissue's original characteristics and functionality (Sheyn et al., 2016).

The osteogenic potential of MSCs involves a highly regulated differentiation program aligning populations of distinct cellular phenotypes regulated by epigenetic mechanisms (Tai et al., 2014). The epigenetic control of gene activity during osteoblastic differentiation is controlled by a complex structural organization involving specific histone methylation/acetylation (Wu et al., 2017). Thus, during the process of MSCs differentiation, transcriptional control of gene expression is fundamental for normal phenotypic development. Histone modifications guarantee chromatin compaction and specific transcriptional epigenetic patterns and are inherited from progenitor cells, thus greatly influencing osteogenic potential and impairment phenotype in regulation during progeny (Hargreaves & Crabtree, 2011; Zhu et al., 2013).

In this scenario, evaluating the molecular and cellular events that occur during osteogenic phenotype commitment from MSCs is very important to map some potential biomarkers, opening strategies to suggest them in biotechnological issues, such as periodontal breakdown. Thus, MSCs obtained from periodontal ligament (PDLCs) have gained a special interest in tissue bioengineering, once they present high proliferative capacity and the ability to recapitulate in vitro the most important and well-defined osteogenic stages, such as proliferation, matrix organization, and mineralization (Seo et al., 2004). However, we must take into account the lessons from the osteogenic phenotype obtained from the differentiation of MSCs into mature osteoblastic cells, where there is a regulation that modulates the expression of the major genes of osteoblast differentiation, RUNX Family Transcription Factor 2 (*RUNX2*) and SP7 transcription factor (*SP7*) (Ducy, Zhang, Geoffroy, Ridall & Karsenty, 1997).

Epigenetically speaking, it is now widely known that numerous enzymes can chemically modify the amino-terminal "tails" of histone proteins, thereby altering the interaction with DNA and allowing interactions with chromodomain and bromodomain-containing proteins that

recognize the lysine acetylation and methylation sites (Bürglin & Affolter, 2016). The regulation of methylation in lysine residues in histones by lysine demethylases (KDMs), has been shown to be important in the commitment of MSCs into osteoblasts (Gordon, Stein, Westendorf & Van Wijnen, 2015). In addition, the enzymes Histone Acetyl Transferase (HAT) and Histone Deacetylase (HDAC) control the acetylation levels of histones and thereby control gene expression (Lakshmaiah, Jacob, Aparna, Lokanatha & Saldanha, 2014).

JARID1B is a JmjC family member, considered as a transcriptional repressor, capable of demethylating the tri- and di-methylated marks of H3K4 (Zeng et al., 2010) and the only member of this family with roles associated to osteoblastic phenotypic acquisition (Rojas et al., 2015). In detail, the lysine demethylase JARID1B mediates the deposition and elimination of histone epitope tags in the P1 promoter during the commitment of MSCs into osteoblastic lineages, therefore, controlling the activation and/or transcriptional repression of the Runx2/p57 (Rojas et al., 2019). Considering the complexity of this mechanism in bone and in line with the above mentioned, the characterization of epigenetic signatures may provide new insights into the involvement of JARID1B in the regulatory mechanisms of genes governing MSCs commitment, especially the *RUNX2/p57* and *SP7* transcriptional control. These findings can be highly relevant and promising to cell therapy and may contribute to identifying new approaches for tissue regeneration and bone disorders comprehension. Here, we aimed to evaluate whether the KDM JARID1B is involved with distinct osteogenic phenotype commitment by considering the heterogeneity of PDLCs for osteoblast differentiation and mineral nodules production.

## MATERIAL AND METHODS

### Cell culture and maintenance

PDLCs with high (h-PDLCs) and low (l-PDLCs) capacity of producing mineral nodules were obtained from healthy third molars from two 20-22-year-old subjects. The consent was obtained from all subjects by the Piracicaba Dental School, University of Campinas and carried out in agreement with a local Ethic Committee's register number: CAAE55588816.4.0000.5418. PDLCs tissue isolation were performed as previously described by Silverio et al., 2010 and cultured in a Dulbecco's Modified Eagle high glucose medium (DMEM) containing 20% fetal bovine serum (FBS), 100 U/mL of penicillin, and 100 mg/mL of streptomycin. All cells were maintained at 37 °C in a humidified atmosphere containing 5% CO2 and all the experiments were realized with cells in the passages P5-P7. The cell viability was determined by the trypan blue dye exclusion test.

**In vitro osteoblast-differentiation model**

l-PDLCs and h-PDLCs (25×104 cells) were seeded into 6-well plates in DMEM medium, containing 10% FBS and antibiotics. After 24 h of incubation at 37 °C in a humidified atmosphere containing 5% CO2, the medium was replaced by osteogenic differentiation medium (OM) (ascorbic acid at 50 μg/mL, β-glycerolphosphate 10 mM, dexamethasone 10 nM) supplemented with 10% FBS and 1% antibiotics for 3 and 10 days (T3 and T10 groups, respectively) under osteogenesis in vitro induction. The control group (T0) was collected on the first day of the osteogenic differentiation induction.

**Global DNA methylation analysis**

For DNA isolation, l-PDLCs and h-PDLCs were cultured at 8.7 x 105 cells per 100 mm dishes in complete culture medium or osteogenic medium, changing the medium every 3 days. Cells were collected at 3rd and 10th days. Two independent experiments were performed. After each period, the culture medium was removed and washed two times with PBS and then, the cells were scrapped off in extraction buffer with proteinase K. Total DNA was purified by extraction with phenol/chloroform/isoamyl alcohol and DNA samples were stored at -20℃. DNA's concentrations and quality were assessed using fluorometers[¶] and spectrophotometer[#].

**Oxidative bisulfite conversion**

The oxidative bisulfite conversion reaction was performed using the oxidative bisulfite conversion kit[**]. Before start, samples were pooled, combining 500 ng of each replicate. Then 1 μg of DNA from pooled samples was purified and denatured. Pooled-DNA from each group was split in two equal reactions, one of which underwent chemical oxidation followed by bisulfite conversion, the other underwent mock oxidation (oxidant replaced by water) followed by bisulfite conversion[††]. All reactions were processed through the array protocol, following manufacturer's guidelines. Array bead chips were scanned[‡‡].

**Data processing**

Beta values represent the measured (hydroxy)methylation values, based on the intensities of probes. Beta values range from 0 to 1 and can be thought of as methylation percentage.

[¶] Qubit; Thermo Fisher Scientific Inc., IL, USA
[#] Nanodrop 1000; Nanodrop Technologies LLC, NC, USA
[**] TrueMethyl oxBS Module; catalog #0414, NuGEN, Tecan Genomics Inc., CA, USA
[††] Infinium Methylation EPIC beadchip; Illumina Inc., CA, USA
[‡‡] HiScanSQ system; Illumina Inc., CA, USA

Processing and statistical analysis of the array data was performed using the R statistical language (Gentleman et al., 2004). The raw idat files produced by Illumina platform were analyzed with minfi package (Aryee et al., 2014), applying SWAN normalization, producing a final data set containing probes and their fold-change values for each sample for further analysis. Genome studio performed quality control test, differentially methylated probes and annotated regions.

**RNA isolation, cDNA synthesis and qPCR conditions**

Total RNA was extracted by TRIzol:chloroform method[§§] and 2 µg of total RNA was used for cDNA synthesis with Superscript II[§§], according to manufacturer's instructions. qPCR was carried out in a total of 20 µL, containing real-time PCR master mix[‖‖] (10 µL), specific primers (5 µM), 60 ng of cDNA and nuclease free H2O in a real-time PCR master mix and thermal cycler[¶¶]. Gene expression was expressed as compared to control cells by ΔΔCT method, using *β-ACTIN*, *RPL19* and *18S* represented on the plate as housekeeping controls. The primers sequence and PCR conditions were expressed in the Table 1.

**Western blotting analysis**

The proteins were extracted in 500 µL Laemmli buffer [SDS 4%, glycerol 20%, Tris-Cl (pH 6.8) 120 mM, bromophenol blue 0.02% (w/v) and DTT 0.1 M]. In short, 15 µL protein (50 mg) was resolved by SDS-PAGE and blotted onto PVDF membranes[##]. Membranes were blocked in Tris-buffered saline (TBS) with 0.05% Tween 20, albumin 2,5% (TBSTA) and incubated overnight at 4°C with appropriate primary antibody for Tri-Methyl-Histone H3 (Lys4)[***] and Histone H3[†††], followed by the appropriate horseradish peroxidase (HRP)-linked secondary antibodies in TBSTA for 1 h an ambient temperature. The immunoreactive bands were detected with enhanced chemiluminescence kit[‡‡‡].

**Statistical analysis**

Results were expressed as mean ± standard deviation. Statistical analysis was performed by the Student's t test or by analysis of variance (ANOVA) followed by the post hoc Tukey

[§§] Invitrogen, Carlsbad, CA, USA
[‖‖] PowerUp™ SYBR™ Green Master Mix 2×; Applied Biosystems, CA, USA
[¶¶] QuantStudio® 3 Real-Time PCR; catalog #A28567, Thermo Fisher Scientific Inc., IL, USA
[##] Immobilon FL; Millipore, Bedford, MA, USA
[***] CST #9727
[†††] CST #9715
[‡‡‡] BIORAD: 1-800-424-6723

test, when more than two groups were compared, using GraphPad Prism 5[§§§]. Differences were considered significant at $p < 0.05$, in two-sided tests of statistical significance.

## RESULTS

### Basal gene expression patterns of *JARID1B*, pluripotency and osteogenic genes differs in PDLCs with distinct capacity of producing mineral nodules

The osteogenic differentiation *in vitro* was performed up to 21 days and PDLCs from different donors responded distinctly to the classical osteogenic induction, which firstly validated the differential behavior of both lineages in mineralizing phenotypes (**Fig. 1a, b**). By now, we distinguish those cells as follows: a cell line presenting higher capacity of producing mineral nodules (high osteogenic potential, h-PDLCs) and other with lower capacity of producing mineral nodules (low osteogenic potential, l-PDLCs), and we explored this condition to better understand the behavior of JARID1B in these both osteogenic phenotypes.

Since the gene expression of *RUNX2*, *RUNX2/p57* and *SP7* are hallmarks of the osteoblast-lineage identity, we first investigated their transcript levels. Our data shows l-PDLCs present reduced basal levels (T0) in the *RUNX2* and *RUNX2/p57* transcripts and an increase in the *SP7* transcript levels, when compared to h-PDLCs (**Fig. 1f, g, h**). In this way, the difference in *RUNX2/p57* and *SP7* basal gene expression observed between both l-PDLCs and h-PDLCs makes clear the repressor effect of JARID1B during the osteoblastic phenotype and it reinforces the functional role for JARID1B in regulating PDLCs cell differentiation, acting as a barrier to the reprogramming process.

Considering the importance of POU5F1-POU-class-5-homeobox-1 (OCT4) and NANOG-Homeobox (NANOG) as transcription factors required to maintain cell pluripotency and undifferentiation state, we also evaluated their basal gene expression in both l-PDLCs and h-PDLCs. As expected, high levels of *OCT4* and *NANOG* transcripts were observed in l-PDLCs (**Fig. 1c, d**). Lastly, we investigated the involvement of JARID1B in osteoblastic phenotype development and our results demonstrated h-PDLCs presenting reduced basal levels (**Fig. 1e**), when compared to l-PDLCs, with significant inversely proportional correlation between the RUNX2 and RUNX2/p57 (**Fig. 1i, j**). Together, this data set validates both l- and h-PDLCs as a tool for studying JARID1B involvement during the molecular steps required in MSCs-acquiring osteogenic phenotype.

[§§§] GraphPad Software Inc., San Diego, CA, EUA

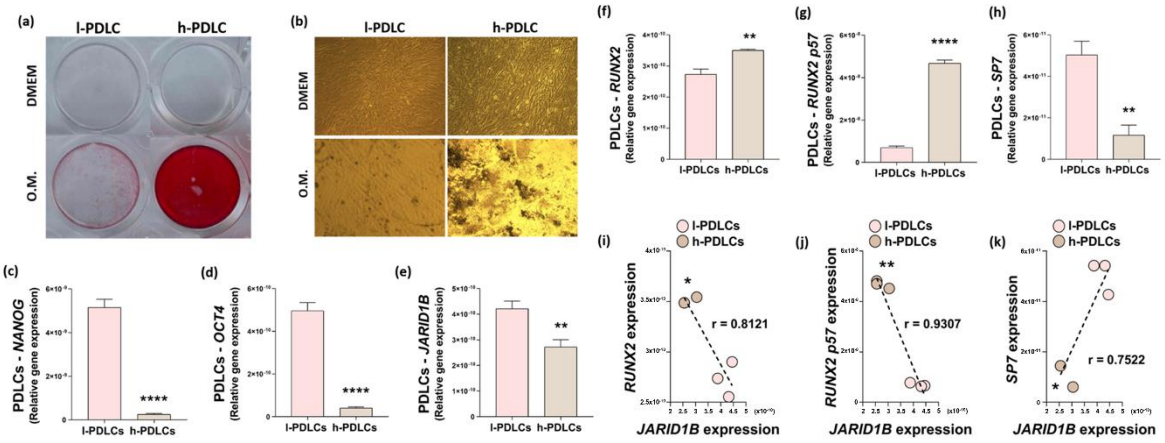


**Figure 1. Basal gene expression patterns of *JARID1B*, pluripotency and osteogenic genes differs in PDLCs com distinct capacity of producing mineral nodules.** (**a**) Alizarin red staining after 21 days of osteogenic induction. (**b**) Representative photomicrographs of in vitro osteogenic differentiation with 10x magnification. *NANOG* (**c**), *OCT4* (**d**), *JARID1B* (**e**), *RUNX2* (**f**), *RUNX2/p57* (**g**) and *SP7* (**h**) gene expression in human mesenchymal stem cells derived from periodontal ligament (PDLCs). Correlation analysis between *JARID1B* versus *RUNX2* (**i**), *RUNX2/p57* (**j**) and *SP7* (**k**) gene expression levels, in PDLCs with low (l-PDLCs) and high (h-PDLCs) osteogenic potential. The relative gene expression levels were determined using the cycle threshold (Ct) method, plotting absolute values in the graphics. The results are represented as mean ± standard deviation of three independent experiments. *p < 0.05, **p < 0.001, ***p < 0.0001 and ****p < 0.00001.

## Differential expression of *RUNX2*, *RUNX2/p57* and *JARID1B* in PDLCs with distinct osteogenic phenotype during osteogenic stimulus

In order to explore the differential expression of *JARID1B*, both l-PDLCs and h-PDLCs were subjected to *in vitro* osteogenic stimulus model for 3 and 10 days. Molecularly, we have investigated whether there were differences between both PDLCs in expressing *RUNX2*, *RUNX2/p57* and *SP7*, and we have now noticed these mRNA profiles remained low in l-PDLCs responding to osteogenic stimulus (**Fig. 2a-c**), except considering *RUNX2* mRNA at 3 days of osteogenic challenge (**Fig. 2a**). Conversely, h-PDLCs show stronger osteogenic potential by significantly up-expressing all those 3 osteogenic biomarkers (**Fig. 2d-f**), reaching approximately 10-fold changes increased of *RUNX2* mRNA levels, compared to T0. Taken these results into account, it is possible to reinforce the potential effect of the epigenetic landscape in modulating the expression of bone-related genes. Thereafter, *NANOG* and *OCT4* genes were also investigated during osteogenic challenge, and our data shows significant down-expression of both genes in l-PDLCs (**Fig. 2g, h**), while h-PDLCs show up-expression of both mRNA patterns at T10 (**Fig. 2j, k**). Later, *JARID1B* mRNA was investigated in this biological model, considering both low and high-osteogenic potential of PDLCs, and our data shows an up-expression of *JARID1B* gene in l-PDLCs at T3 and down-expression at T10 (**Fig. 2i**), while an opposite result was found by h-PDLCs (**Fig. 2l**).

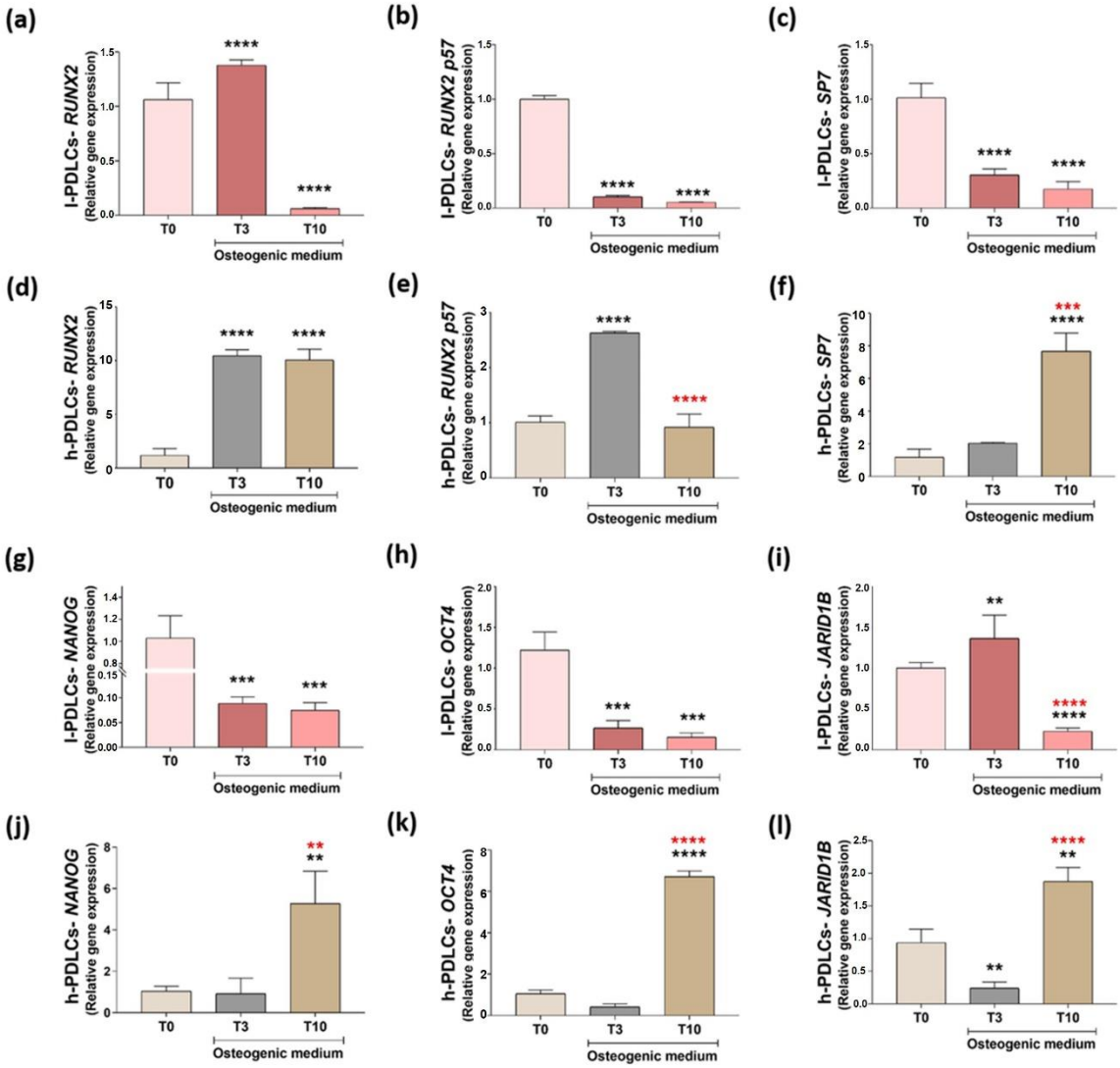


**Figure 2. Differential expression of *RUNX2*, *RUNX2/p57* and *JARID1B* in PDLCs with distinct osteogenic phenotype during osteogenic stimulus.** qPCR analysis of *RUNX2* (**a, d**), *RUNX2/p57* (**b, e**), *SP7* (**c, f**), *NANOG* (**g, j**), *OCT4* (**h, k**) and *JARID1B* (**i, l**) of human mesenchymal stem cells derived from periodontal ligament (PDLCs), after 3 and 10 days of osteogenic stimulus. The relative gene expression levels were determined using the cycle threshold (Ct) method, plotting absolute values in the graphics. The results represented as mean ± standard deviation of three independent experiments. *p < 0.05, **p < 0.001, ***p < 0.0001 and ****p < 0.00001. * when compared with T0 group and * when compared with T3 group.

## l- and h-PDLCs present distinct patterns of DNA (hydroxy)methylation in the *JARID1B* gene, during osteogenic differentiation

The probes identified for *JARID1B* gene (n=45) presented lower AVG_Beta intensities of 5-meC and hypomethylated pattern in l-PDLCs compared to h-PDLCs, in both T3 and T10 groups (**Fig. 3a, b**). The percentage of differentiated methylated probes (DMPs) was 11% hypomethylated in T3 and 33% hypomethylated and 5% hypermethylated in T10 (**Fig. 3c**). The DMP's annotation was predominant in promoter (TSS1500 and TSS200), 1st exon and 3'UTR

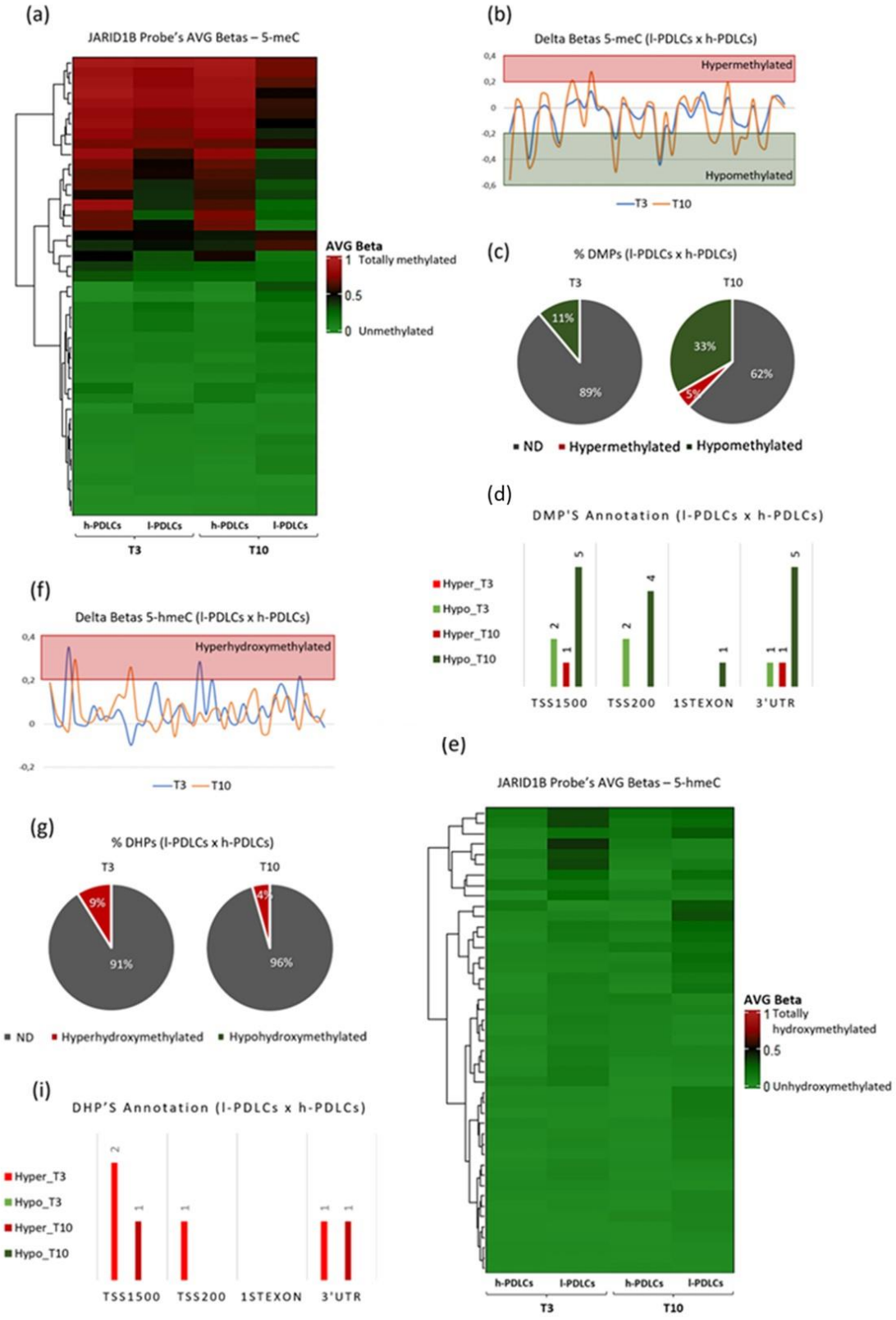


**Figure 3.** ***JARID1B*** **(Hydroxy)Methylation Patterns in T3 and T10 groups.** (**a, e**) The heatmaps represent the average beta values (AVG Betas) to methylation (5-meC) and hydroxymethylation (5-hmeC) of the probes detected to *JARID1B* gene (#45). (**b, f**) The scatter plots show the 5-meC and 5-hmeC delta betas between l-PDLCs and h-PDLCs probes. (**c, g**) The pie charts represent the percentage of differently methylated (DMPs) and hydroxymethylated (DHPs) probes in l-PDLCs (x h-PDLCs). (**d, h**) – The bar graphs show the DMP's and DHP's annotation (l-PDLCs x h-PDLCs), according to *GENCODECOMPV12_GROUP* reference.

gene regions (**Fig. 3d**). In contrast, the AVG_Beta intensities of 5-hmeC were higher in l-PDLCs, presenting hyperhydroxymethylated pattern, when compared to h-PDLCs, in both T3 and T10 groups (**Fig. 3e, f**), which favor the more permissive chromatin in those regions. The percentage of differently hydroxymethylated probes (DHPs) was 9% and 4% hyperhydroxymethylated in T3 and T10, respectively (**Fig. 3g**). The DHP's annotation was predominant in promoter and 3'UTR gene regions (**Fig. 3h**).

## Negative modulation of *RUNX2/p57* gene expression is correlated with high levels of *JARID1B* transcripts

Pearson's correlation analysis shows statistical significance for *RUNX2/p57* gene expression (r > 0.96) for l-PDLCs, at 3 days of osteogenic stimulus (**Fig. 4b**). At the same time, *JARID1B* gene expression is correlated with *RUNX2* (r = 0.9514), *RUNX2/p57* (r = 0.9738) and *SP7* (r = 0.9738) gene expression for h-PDLCs (**Fig. 4d-f**).

We have also applied this strategy at 10 days of PDLCs responding to osteogenic stimulus and significant correlations were observed for *JARID1B* gene expression versus *RUNX2* (**Fig. 4g**), *RUNX2/p57* (**Fig. 4h**) and *SP7* (**Fig. 4i**) mRNA patterns, only in l-PDLCs.

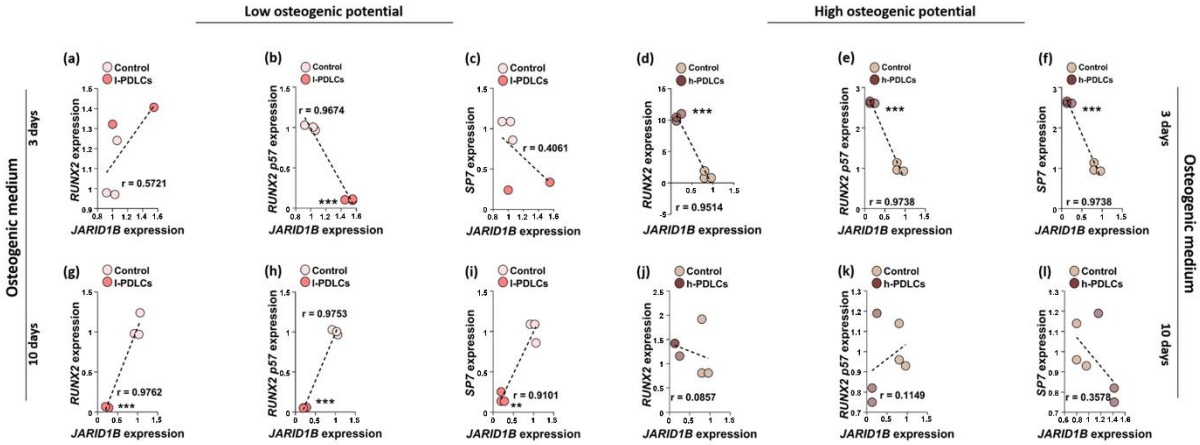


**Figure 4. Negative modulation of *RUNX2/p57* gene expression is correlated with high levels of *JARID1B* transcripts.** Correlation analysis between *JARID1B* versus *RUNX2* (**a, d, g, j**), *RUNX2/p57* (**b, e, h, k**) and *SP7* (**c, f, i, l**) gene expression levels, in PDLCs with low (l-PDLCs) and high (h-PDLCs) osteogenic potential, after 3 and 10 days of osteogenic induction. Results were represented as mean ± standard deviation of three independent experiments. *p < 0.05, **p < 0.001 and ***p < 0.0001. Significant positive correlation between r = 0.683 and 1.

## Global H3K4 methylation is modulated in PDLCs presenting distinct osteogenic phenotypes

At 3 days, immunoblotting data reveals a significant reduction in the global H3K4me3 content only in h-PDLCs, while an increase was observed for both PDLCs, at 10 days of

osteogenic stimulus (**Fig. 5a-d**), being this increase much higher in h-PDLCs than in l-PDLCs, when we compare T3 x T10 from both PDLCs and even when we compare h-PDLCs and l-PDLCs at 10 days (**Fig. 5c, d**).

However, some inversely proportional correlations, between global H3K4me3 levels and *JARID1B* gene expression with a Pearson's product moment above r = 0.8776 were observed for l-PDLCs, at 10 days (**Fig. 5f**). Conversely, the correlations observed in the h-PDLCs were not inversely proportional (**Fig. 5g, h**).

In addition, the correlations between the global H3K4me3 levels and the osteogenic markers transcripts were inversely proportional with an increase in the global H3K4me3 levels and decrease in the *RUNX2*, *RUNX2/p57* and *SP7* gene expression, at 10 days considering l-PDLCs (**Fig. 5l, m, n**). Contrary, the results in the h-PDLCs show the increase in the gene expression of the osteoblastic gene markers was accompanied by the global H3K4me3 level reduction (**Fig. 5o, p, q**), at 3 days. In addition, a positive correlation for *RUNX2* and *SP7* genes was observed at 10 days of osteogenic stimulus (**Fig. 5r, t**).

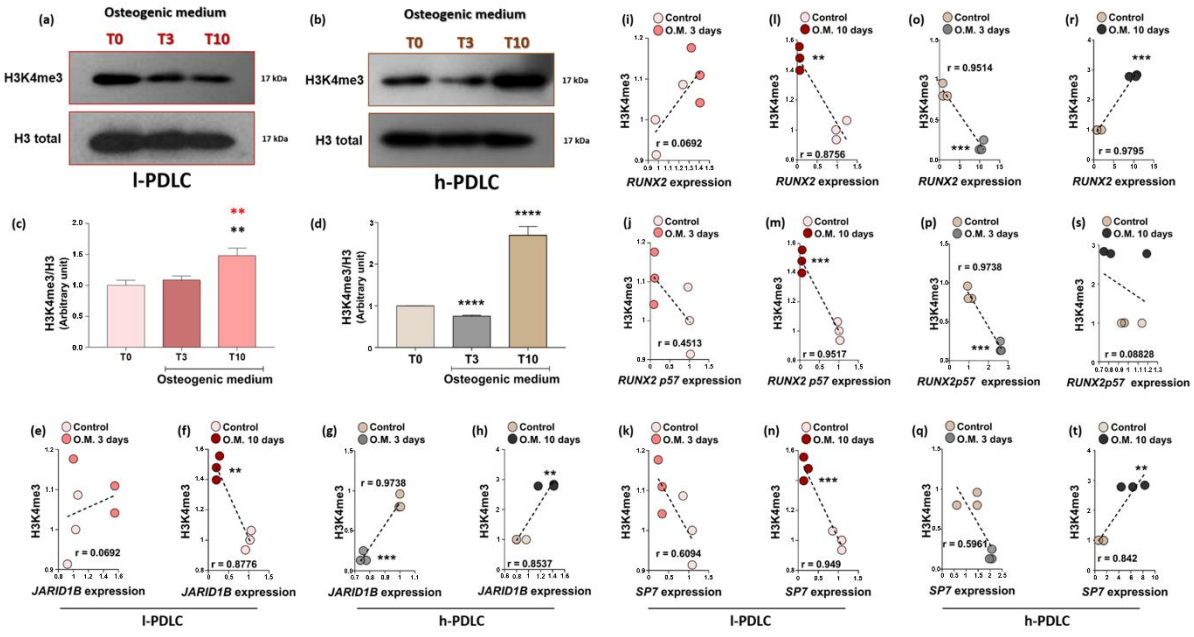


**Figure 5. Global H3K4 methylation is modulated in PDLCs presenting distinct osteogenic phenotypes.** Immunoblot of whole cell extracts from l-PDLCs (**a**) and h-PDLCs (**b**) using antibodies against H3K4me3 and H3. (**c, d**) Densitometric analysis of immunoblots was measured using the ImageJ Software normalized to the protein ratio of controls, which were normalized by 1, with H3 as loading control. Correlation analysis between global H3K4me3 levels versus *JARID1B* expression (**e-h**), global H3K4me3 levels with *RUNX2* expression (**i-r**), *RUNX2/p57* (**j-s**) and SP7 (**k-t**). Results were represented as mean ± standard deviation of three independent experiments. **p < 0.001, ***p < 0.0001 and ***p < 0.0001. Significant positive correlation between r = 0.683 and 1.

## DISCUSSION

The main results of this study indicate a crucial role of JARID1B in repressing PDLCs osteogenic phenotype, proposing JARID1B as a potential therapeutic target for periodontal and bone regeneration. Despite the advances in regenerative therapies based on stem cells, some issues still need to be elucidated. An important point this study aims to answer is when the patient presents PDLCs with low osteogenic potential, which could compromise the results of using their cells to correct bone and/or periodontal defects. Therefore, our findings suggest that JARID1B silencing could promote a better osteogenic potential, bringing more promising results for bone regeneration of periodontal and/or bone defects.

It is known that RUNX2 is a transcription factor controlling bone development, and its epigenetic regulation is required to better understand osteoblast differentiation and potential bone disorders. A previous publication showed JARID1B as a key epigenetic component in modulating mesenchymal cell fate into osteogenic lineage by regulating *RUNX2* gene activity (Rojas et al., 2015). Now, we have focused on evaluating the importance of JARID1B on contributing to the osteogenic phenotype by considering non-transfected PDLCs, from two different donors, which present low and high osteogenic potential. It is tempting to assume that understanding the regulation of PDLCs during osteogenesis will contribute, in the near future, to the development of clinical trials of cell therapy in humans.

Herein, we found higher basal levels of *OCT4* and *NANOG* in the l-PDLCs, compared to h-PDLCs, which agrees with previous publications from our group (Assis et al., 2021; Ferreira et al., 2022). Both, *OCT4* and *NANOG* genes are expressed in MSCs (Greco, Liu & Rameshwar, 2007; Wei & Shen, 2011) and constitute the core network that regulates and suppresses differentiation-associated genes. In this sense, they are involved in keeping the state of non-differentiation and multipotentiality of cells and could be, at least in part, related to lower levels of producing mineral nodules.

Additionally, our results also showed l-PDLCs expressing higher basal levels of *JARID1B*, compared to h-PDLCs, with significant inversely proportional correlations between the *RUNX2* and *RUNX2/p57*. This data set validates both h- and l-PDLCs as a tool for studying JARID1B involvement during the molecular steps required in MSCs-acquiring osteogenic phenotype. In fact, we have reinforced the relevance of JARID1B in negatively modulating the bone-master *RUNX2* gene, and it might explain that JARID1B levels are sufficient to maintain the *RUNX2* repression in myoblasts (Rojas et al., 2015).

When submitted to an osteogenic environment, PDLCs express several bone biomarkers. Thus, to explore the differential expression of *JARID1B*, both l-PDLCs and h-PDLCs were

subjected to in vitro osteogenic stimulus model for 3 and 10 days. Molecularly, we have investigated whether there were differences between both PDLCS in expressing *RUNX2*, *RUNX2/p57* and *SP7* genes, and we have now noticed these mRNA profiles remained low in l-PDLCs during the osteogenic stimulus, except *RUNX2* mRNA at three days. On the other hand, h-PDLCs showed stronger osteogenic potential by significantly up-expressing all three osteogenic biomarkers, reaching approximately 10-fold changes in mRNA *RUNX2*, compared with T0 (unchallenged cells). Therefore, it is possible to suggest the potential effect of the epigenetic landscape in modulating the expression of bone-related genes. Further, our data show significant down-expression of *NANOG* and *OCT4* genes in challenged l- PDLCs, while h-PDLCs show up-expression of both mRNA patterns at T10. Next, *JARID1B* mRNA was investigated in this biological model, considering both the low and high-osteogenic potential of PDLCs. The results showed an up-expression of JARID1B gene in l-PDLCs at T3 and down-expression at T10, while the opposite result was found by h-PDLCs.

LSD1 was the first histone demethylase to be discovered, with action on H3K4 marker; however, LSD1 has been shown to be a component of both the repressing and activating complexes (Metzger et al., 2005) . On the other hand, the member of the JmjC family (JARID1A, JARID1B, JARID1C and JARID1D) are capable of demethylating the tri- and di-methylated marks of H3K4 (Zeng et al., 2010) and have traditionally been considered transcriptional repressors, since can catalyze the removal of H3K4 methylation (H3K4me3, H3K4me2), which is predominantly found in promoters of actively transcribed genes (Xhabija & Kidder, 2019). Interestingly, only JARID1B had its function demonstrated during osteoblastic phenotypic acquisition (Rojas et al., 2015). In order to better understand the epigenetic background of *JARID1B* gene, we first analyzed its (hydroxy)methylation pattern in the Methylome dataset. The probes identified for *JARID1B* gene presented a hypomethylated pattern in l-PDLCs compared to h-PDLCs, in both T3 and T10, being predominantly in TSS1500 and TSS200, 1st exon and 3'UTR gene regions. In addition, l-PDLCs also presented hydroxymethylated patterns stronger than h-PDLCs, in both T3 and T10, being predominant in promoter and 3'UTR gene regions. Interestingly, the increase of hypomethylated probes in l-PDLCs (x h-PDLCs) from T3 to T10 (three times greater) was correlated with the decrease of hyperhydroxymethylated probes in the same groups (2 times smaller), indicating a possible epigenetic regulation on *JARID1B* gene, mediated by DNA methyltransferases (DNMTs) and ten-eleven translocation (TETs) enzymes, which are agents of methylation and hydroxymethylation. However, this must be further investigated in the future. Altogether, these results show an epigenetic status more favorable to *JARID1B* expression in l-PDLCs, compared to h-PDLCs, during osteogenic differentiation.

Considering l-PDLCs present high levels of *JARID1B* transcripts, we decided to further analyze the correlation between the *JARID1B* gene expression and the levels of osteogenic gene markers in both low and high PDLCs, under the osteogenic stimulus. Pearson's correlation analysis showed significance for *RUNX2/p57* gene expression for l-PDLCs, and, additionally, *JARID1B* gene expression was also correlated with *RUNX2*, *RUNX2/p57* and *SP7* gene expression for h-PDLCs, at 3 days responding to osteogenic stimulus. Moreover, we applied this strategy at 10 days of PDLCs responding to osteogenic stimulus and significant correlations were observed for *JARID1B* gene expression versus *RUNX2*, *RUNX2/p57* and *SP7* mRNA patterns only in l-PDLCs. These data indicate that *JARID1B* gene expression is important in the osteogenic potential commitment and phenotype determination from MSCs. In addition, it has been shown that JARID1B plays an important role in myogenic lineage specification from MSCs, by regulating the enrichment of H3K4me3 at the *RUNX2* gene promoter (Rojas et al., 2015). In this study, the authors demonstrated that *JARID1B* silencing prevents the repression of the *RUNX2* P1 promoter (RUNX2/p57) during myogenic differentiation of MSCs, identifying JARID1B as a key component of a potent epigenetic switch responsible for controlling the fate of MSCs in myogenic and osteogenic lineages, acting as a barrier to the reprogramming process.

To evaluate H3K4 methylation during the osteogenic phenotype, we analyzed trimethylation levels in l-PDLCs and h-PDLCs, responding to osteogenic stimulus, and considering the two time points 3 and 10 days. Firstly, immunoblotting data reveals a significant reduction in the global H3K4me3 content only in h-PDLCs, at 3 days, with an increase in the global H3K4me3 content at 10 days, for both PDLCs. However, inversely proportional correlations between global H3K4me3 levels and *JARID1B* gene expression were observed for l-PDLCs, at 10 days. Conversely, the correlations observed in h-PDLCs were not inversely proportional. Biochemically, H3K4me3 mediates more efficiently the induction of gene expression in response to environmental signals (Atlasi & Stunnenberg, 2017; Tan et al., 2014; Vermeulen et al., 2010; Vastenhouw et al., 2010). Our results show that the overall expression of H3K4me3 was decreased only during the initial phase of osteoblastic differentiation (3 days) in h-PDLCs, suggesting the osteoblastic phenotype from MSCs is accompanied by the loss of H3K4me3 at global levels. This fact is directly related to the level of expression of *JARID1B*, since histone demethylase is the enzyme responsible for the demethylation of H3K4me3 and repression of genes responsible for the maintenance of pluripotency during the speciation of stem cells (Kidder, Hu, Yu, Liu & Zhao, 2013).

Notably, h-PDLCs showed an increase in the osteoblastic gene markers' gene expression, accompanied by a decrease in the global H3K4me3 levels, only at 3 days. After this period, the correlations were not inverse anymore, as observe in l-PDLCs, in which the correlations between global H3K4me3 levels and osteogenic markers transcripts were inversely proportional, at 10 days.

## CONCLUSION

Taking into consideration the limitations of this study, our results show the crucial role of JARID1B in repressing PDLCs osteogenic phenotype, and this opens the necessity to better understand the behavior of this gene in bone disorders that compromise the osteoblast performance, proposing JARID1B as a potential therapeutic target for periodontal regeneration.

## ACKNOWLEDGMENTS

This work was supported by São Paulo Research Foundation – FAPESP (grant numbers: 2013/09650-8, 2014/22689-3, 2016/08888-9 and 2018/10443-0) and Higher Education Personnel Improvement Coordination (Brazil) – CAPES (financing code: 001).

## CONFLICT OF INTERESTS

The authors declare no competing financial interests.

## ORCID

Rogério S. Ferreira – 0000-0003-1090-7442

Rodrigo A. da Silva - 0000-0002-7754-1855

Geórgia da S. Feltran - 0000-0002-5743-5182

Ericka Patricia da Silva - 0000-0002-4573-2921

Rahyza I. F. Assis - 0000-0003-3068-5728

Emanuel Silva Rovai - 0000-0002-5044-0368

Willian F. Zambuzzi - 0000-0002-4149-5965

Denise C. Andia - 0000-0002-0049-0201

REFERENCES

Aryee, M. J., Jaffe, A. E., Corrada-Bravo, H., Ladd-Acosta, C., Feinberg, A. P., Hansen, K. D., & Irizarry, R. A. (2014). Minfi: a flexible and comprehensive Bioconductor package for the analysis of Infinium DNA methylation microarrays. *Bioinformatics*, *30*(10), 1363-1369. https://doi.org/10.1093/bioinformatics/btu049.

Assis, R. I., Schmidt, A. G., Racca, F., da Silva, R. A., Zambuzzi, W. F., Silvério, K. G., ... & Andia, D. C. (2021). DNMT1 inhibitor restores RUNX2 expression and mineralization in periodontal ligament cells. *DNA and Cell Biology*, *40*(5), 662-674. https://doi.org/10.1089/dna.2020.6239.

Atlasi, Y., & Stunnenberg, H. G. (2017). The interplay of epigenetic marks during stem cell differentiation and development. *Nature Reviews Genetics*, *18*(11), 643-658. https://doi.org/10.1038/nrg.2017.57.

Baroncelli, M., Fuhler, G. M., Van de Peppel, J., Zambuzzi, W. F., van Leeuwen, J. P., van der Eerden, B. C., & Peppelenbosch, M. P. (2019). Human mesenchymal stromal cells in adhesion to cell-derived extracellular matrix and titanium: Comparative kinome profile analysis. *Journal of Cellular Physiology*, *234*(3), 2984-2996. https://doi.org/10.1002/jcp.27116.

Bürglin, T. R., & Affolter, M. (2016). Homeodomain proteins: an update. *Chromosoma*, *125*(3), 497-521. https://doi.org/10.1007/s00412-015-0543-8.

Cho, T. J., Gerstenfeld, L. C., & Einhorn, T. A. (2002). Differential temporal expression of members of the transforming growth factor β superfamily during murine fracture healing. *Journal of bone and mineral research*, *17*(3), 513-520. https://doi.org/10.1359/jbmr.2002.17.3.513.

Ducy, P., Zhang, R., Geoffroy, V., Ridall, A. L., & Karsenty, G. (1997). Osf2/Cbfa1: a transcriptional activator of osteoblast differentiation. *cell*, *89*(5), 747-754. https://doi.org/10.1016/S0092-8674(00)80257-3.

Ferreira, R. S., Assis, R. I., Feltran, G. D. S., do Rosário Palma, I. C., Françoso, B. G., Zambuzzi, W. F., ... & da Silva, R. A. (2022). Genome-wide DNA (hydroxy) methylation reveals the individual epigenetic landscape importance on osteogenic phenotype acquisition in

periodontal ligament cells. *Journal of periodontology*, *93*(3), 435-448. https://doi.org/10.1002/JPER.21-0218.

Gentleman, R. C., Carey, V. J., Bates, D. M., Bolstad, B., Dettling, M., Dudoit, S., ... & Zhang, J. (2004). Bioconductor: open software development for computational biology and bioinformatics. *Genome biology*, *5*(10), 1-16. https://doi.org/10.1186/gb-2004-5-10-r80.

Gordon, J. A., Stein, J. L., Westendorf, J. J., & Van Wijnen, A. J. (2015). Chromatin modifiers and histone modifications in bone formation, regeneration, and therapeutic intervention for bone-related disease. *Bone*, *81*, 739-745. https://doi.org/10.1016/j.bone.2015.03.011.

Greco, S. J., Liu, K., & Rameshwar, P. (2007). Functional similarities among genes regulated by OCT4 in human mesenchymal and embryonic stem cells. *Stem cells*, *25*(12), 3143-3154. https://doi.org/10.1634/stemcells.2007-0351.

Hargreaves, D. C., & Crabtree, G. R. (2011). ATP-dependent chromatin remodeling: genetics, genomics and mechanisms. *Cell research*, *21*(3), 396-420. https://doi.org/10.1038/cr.2011.32.

Kidder, B. L., Hu, G., Yu, Z. X., Liu, C., & Zhao, K. (2013). Extended self-renewal and accelerated reprogramming in the absence of Kdm5b. *Molecular and cellular biology*, *33*(24), 4793-4810. https://doi.org/10.1128/MCB.00692-13.

Lakshmaiah, K. C., Jacob, L. A., Aparna, S., Lokanatha, D., & Saldanha, S. C. (2014). Epigenetic therapy of cancer with histone deacetylase inhibitors. *Journal of cancer research and therapeutics*, *10*(3), 469-478. https://doi.org/10.4103/0973-1482.137937.

Metzger, E., Wissmann, M., Yin, N., Müller, J. M., Schneider, R., Peters, A. H., ... & Schüle, R. (2005). LSD1 demethylates repressive histone marks to promote androgen-receptor-dependent transcription. *Nature*, *437*(7057), 436-439. https://doi.org/10.1038/nature04020.

Rojas, A., Aguilar, R., Henriquez, B., Lian, J. B., Stein, J. L., Stein, G. S., ... & Montecino, M. (2015). Epigenetic control of the bone-master Runx2 gene during osteoblast-lineage commitment by the histone demethylase JARID1B/KDM5B. *Journal of biological chemistry*, *290*(47), 28329-28342. https://doi.org/10.1074/jbc.M115.657825.

Rojas, A., Sepulveda, H., Henriquez, B., Aguilar, R., Opazo, T., Nardocci, G., ... & Montecino, M. (2019). Mll-COMPASS complexes mediate H3K4me3 enrichment and transcription of the

osteoblast master gene Runx2/p57 in osteoblasts. *Journal of cellular physiology*, *234*(5), 6244-6253. https://doi.org/10.1002/jcp.27355.

Rux, D. R., Song, J. Y., Pineault, K. M., Mandair, G. S., Swinehart, I. T., Schlientz, A. J., ... & Wellik, D. M. (2017). Hox11 function is required for region-specific fracture repair. *Journal of Bone and Mineral Research*, *32*(8), 1750-1760. https://doi.org/10.1002/jbmr.3166.

Seo, B. M., Miura, M., Gronthos, S., Bartold, P. M., Batouli, S., Brahim, J., ... & Shi, S. (2004). Investigation of multipotent postnatal stem cells from human periodontal ligament. *The Lancet*, *364*(9429), 149-155. https://doi.org/10.1016/S0140-6736(04)16627-0.

Sheyn, D., Ben-David, S., Shapiro, G., De Mel, S., Bez, M., Ornelas, L., ... & Gazit, Z. (2016). Human induced pluripotent stem cells differentiate into functional mesenchymal stem cells and repair bone defects. *Stem cells translational medicine*, *5*(11), 1447-1460. https://doi.org/10.5966/sctm.2015-0311.

Silvério, K. G., Rodrigues, T. L., Coletta, R. D., Benevides, L., Da Silva, J. S., Casati, M. Z., ... & Nociti Jr, F. H. (2010). Mesenchymal stem cell properties of periodontal ligament cells from deciduous and permanent teeth. *Journal of periodontology*, *81*(8), 1207-1215. https://doi.org/10.1902/jop.2010.090729.

Tai, P. W., Wu, H., Gordon, J. A., Whitfield, T. W., Barutcu, A. R., Van Wijnen, A. J., ... & Stein, J. L. (2014). Epigenetic landscape during osteoblastogenesis defines a differentiation-dependent Runx2 promoter region. *Gene*, *550*(1), 1-9. https://doi.org/10.1016/j.gene.2014.05.044.

Tan, J. Y., Vance, K. W., Varela, M. A., Sirey, T., Watson, L. M., Curtis, H. J., ... & Marques, A. C. (2014). Cross-talking noncoding RNAs contribute to cell-specific neurodegeneration in SCA7. *Nature structural & molecular biology*, *21*(11), 955-961. https://doi.org/10.1038/nsmb.2902.

Vastenhouw, N. L., Zhang, Y., Woods, I. G., Imam, F., Regev, A., Liu, X. S., ... & Schier, A. F. (2010). Chromatin signature of embryonic pluripotency is established during genome activation. *Nature*, *464*(7290), 922-926. https://doi.org/10.1038/nature08866.Wei, X., & Shen, C. Y. (2011). Transcriptional regulation of oct4 in human bone marrow mesenchymal stem cells. *Stem cells and development*, *20*(3), 441-449. https://doi.org/10.1089/scd.2010.0069.

Vermeulen, M., Eberl, H. C., Matarese, F., Marks, H., Denissov, S., Butter, F., ... & Mann, M. (2010). Quantitative interaction proteomics and genome-wide profiling of epigenetic histone marks and their readers. *Cell*, *142*(6), 967-980. https://doi.org/10.1016/j.cell.2010.08.020.

Wu, H., Gordon, J. A., Whitfield, T. W., Tai, P. W., van Wijnen, A. J., Stein, J. L., ... & Lian, J. B. (2017). Chromatin dynamics regulate mesenchymal stem cell lineage specification and differentiation to osteogenesis. *Biochimica et Biophysica Acta (BBA)-Gene Regulatory Mechanisms*, *1860*(4), 438-449. https://doi.org/10.1016/j.bbagrm.2017.01.003.

Xhabija, B., & Kidder, B. L. (2019, August). KDM5B is a master regulator of the H3K4-methylome in stem cells, development and cancer. In *Seminars in cancer biology* (Vol. 57, pp. 79-85). Academic Press. https://doi.org/10.1016/j.semcancer.2018.11.001.

Zeng, J., Ge, Z., Wang, L., Li, Q., Wang, N., Björkholm, M., ... & Xu, D. (2010). The histone demethylase RBP2 Is overexpressed in gastric cancer and its inhibition triggers senescence of cancer cells. *Gastroenterology*, *138*(3), 981-992. https://doi.org/10.1053/j.gastro.2009.10.004.

Zhu, J., Adli, M., Zou, J. Y., Verstappen, G., Coyne, M., Zhang, X., ... & Bernstein, B. E. (2013). Genome-wide chromatin state transitions associated with developmental and environmental cues. *Cell*, *152*(3), 642-654. https://doi.org/10.1016/j.cell.2012.12.033.

**Table S1: Primers sequences and qPCR cycle conditions.**

| Gene (ID) | Primers | 5'- 3' Sequence | Reaction conditions | Product size (bp) |
|---|---|---|---|---|
| *OCT4* (5460) | Forward | GAA ATC CGA AGC CAG GTG TC | 95°C - 15s; 62°C - 30s; 72°C - 30s | 194 |
| | Reverse | TCC TTC GCC TCA GTT TCT CC | | |
| *NANOG* (79923) | Forward | CGA GAC ATA GAC TAT CTG CCT GA | 95°C - 15s; 60°C - 30s; 72°C - 30s | 103 |
| | Reverse | TTC TTC TCA GAC TAC CAT TCC G | | |
| *RUNX2* (860) | Forward | CCG TCC ATC CAC TCT ACC AC | 95°C - 15s; 57°C - 30s; 72°C - 30s | 289 |
| | Reverse | ATG AAA TGC TTG GGA ACT GC | | |
| *RUNX2* p57 (860) | Forward | GGT TAA TCT CCG CAG GTC AC | 95°C - 15s; 55.5°C - 30s; 72°C - 15s | 345 |
| | Reverse | GTC ACT GTG CTG AAG GGA CT | | |
| *SP7* (121340) | Forward | CCA GGC AAC ACT CCT ACT CC | 95°C - 15s; 59°C - 30s; 72°C - 30s | 473 |
| | Reverse | GCC TTG CCA TAC ACCT TGC | | |
| JARID1B (10765) | Forward | TCC CAG GAG GAC ATT ATT GC | 95°C - 15s; 55.5°C - 30s; 72°C - 15s | 203 |
| | Reverse | CCT GCC TGA AAA ATG TGG TT | | |
| *GAPDH* (2597) | Forward | AAG GTG AAG GTC GGA GTC AA | 95°C – 10s; 58°C – 30s; 72°C – 30s | 345 |
| | Reverse | AAT GAA GGG GTC ATT GAT GG | | |
| *β–ACTINA* (60) | Forward | GCA CAG AGC CTC GCC TT | 95°C – 10s; 58°C – 30s; 72°C – 30s | 253 |
| | Reverse | GTT GTC GAC GAC GAG CG | | |
| *18S* (100008588) | Forward | CGG ACA GGA TTGACA GAT TGA TAG C | 95°C – 10s; 60°C – 30s; 72°C – 30s | 118 |
| | Reverse | TGC CAG AGT CTC GTT CGT TAT CG | | |

## 4. CONCLUSÃO GERAL

Juntos, os resultados dos 2 artigos indicam a histona desmetilase JARID1B e os lncRNAs MIR31HG e LINC00939 como possíveis reguladores epigenéticos no comprometimento osteogênico das l-PDLCs.

## REFERÊNCIAS


1. Armitage GC, Xenoudi P. Post-treatment supportive care for the natural dentition and dental implants. Periodontology 2000. 2016;71(1):164-184.

2. Wilder RS, Bray KS. Improving periodontal outcomes: merging clinical and behavioral science. Periodontology 2000. 2016;71(1):65-81.

3. Graziani F, Karapetsa D, Alonso B, Herrera D. Nonsurgical and surgical treatment of periodontitis: how many options for one disease?. Periodontology 2000. 2017;75(1):152-188.

4. Renvert S, Polyzois I. Treatment of pathologic peri-implant pockets. Periodontology 2000. 2018;76(1):180-190.

5. Tsuchida S, Nakayama T. Recent Clinical Treatment and Basic Research on the Alveolar Bone. Biomedicines. 2023;11(3):843.

6. Tassi SA, Sergio NZ, Misawa MYO, Villar CC. Efficacy of stem cells on periodontal regeneration: systematic review of pre-clinical studies. Journal of Periodontal Research. 2017;52(5):793-812.

7. Dominici MLBK, Le Blanc K, Mueller I, Slaper-Cortenbach I, Marini FC, Krause DS, et al. Minimal criteria for defining multipotent mesenchymal stromal cells. The International Society for Cellular Therapy position statement. Cytotherapy. 2006;8(4):315-317.

8. Hargreaves KM, Diogenes A, Teixeira FB. Treatment options: biological basis of regenerative endodontic procedures. Pediatric dentistry. 2013;35(2):129-140.

9. Saito MT, Salmon CR, Amorim BR, Ambrosano GM, Casati MZ, Sallum EA, et al. Characterization of highly osteoblast/cementoblast cell clones from a CD105-enriched periodontal ligament progenitor cell population. J Periodontol. 2014;85(6):e205-11.

10. Ferreira RS, Assis RI, Feltran GDS, do Rosário Palma IC, Françoso BG, Zambuzzi WF, et al. Genome-wide DNA (hydroxy) methylation reveals the individual epigenetic landscape importance on osteogenic phenotype acquisition in periodontal ligament cells. J. Periodontol. 2022;93:435-448.

11. Assis RI, Racca F, Ferreira RS, Ruiz KG, da Silva RA, Clokie SJ, et al. Osteogenic commitment of human periodontal ligament cells is predetermined by methylation, chromatin accessibility and expression of key transcription factors. Cells. 2022;11(7):1126.

12. Amarasekara DS, Kim S, Rho J. Regulation of Osteoblast Differentiation by Cytokine Networks. International Journal of Molecular Sciences. 2021;22(6):2851.

13. Al Aboud NM, Tupper C, Jialal I. Genetics, epigenetic mechanism. 2018

14. Shi YG, Tsukada Y. The discovery of histone demethylases. Cold Spring Harb Perspect Biol. 2013;5(9):a017947.

15. Rojas A, Aguilar R, Henriquez B, Lian JB, Stein JL, Stein GS, et al. Epigenetic control of the bone-master Runx2 gene during osteoblast-lineage commitment by the histone demethylase JARID1B/KDM5B. Journal of biological chemistry. 2015;290(47):28329-28342.

16. Moore LD, Le T, Fan G. DNA methylation and its basic function. Neuropsychopharmacology. 2013;38(1):23-38.

17. Pratt AJ, MacRae IJ. The RNA-induced silencing complex: a versatile gene-silencing machine. J. Biol. Chem. 2009;284(27):17897-17901.

18. Statello L, Guo CJ, Chen LL, Huarte M. Gene regulation by long non-coding RNAs and its biological functions. Nat. Rev. Mol. Cell Biol. 2021;22(2):96-118.